Corrections

PHARMACOLOGY

Correction for "Targeting the minor pocket of C5aR for the rational design of an oral allosteric inhibitor for inflammatory and neuropathic pain relief," by Alessio Moriconi, Thiago M. Cunha, Guilherme R. Souza, Alexandre H. Lopes, Fernando Q. Cunha, Victor L. Carneiro, Larissa G. Pinto, Laura Brandolini, Andrea Aramini, Cinzia Bizzarri, Gianluca Bianchini, Andrea R. Beccari, Marco Fanton, Agostino Bruno, Gabriele Costantino, Riccardo Bertini, Emanuela Galliera, Massimo Locati, Sérgio H. Ferreira, Mauro M. Teixeira, and Marcello Allegretti, which appeared in issue 47, November 25, 2014, of *Proc Natl Acad Sci USA* (111:16937–16942; first published November 10, 2014; 10.1073/pnas.1417365111).

The authors note that an additional affiliation should be listed for Emanuela Galliera. This author's affiliations should appear as "Department of Biomedical, Surgical and Dental Sciences, University of Milan, I-20133 Milan, Italy; and Istituto di Ricerca e Cura a Carattere Scientifico (IRCCS) Galeazzi Orthopaedic Institute, I-20161 Milan, Italy." The corrected author and affiliation lines appear below. The online version has been corrected.

Alessio Moriconi[a,1], Thiago M. Cunha[b,1], Guilherme R. Souza[b], Alexandre H. Lopes[b], Fernando Q. Cunha[b], Victor L. Carneiro[b], Larissa G. Pinto[b], Laura Brandolini[a], Andrea Aramini[a], Cinzia Bizzarri[a], Gianluca Bianchini[a], Andrea R. Beccari[a], Marco Fanton[a], Agostino Bruno[c], Gabriele Costantino[c], Riccardo Bertini[d], Emanuela Galliera[e,f], Massimo Locati[g,h], Sérgio H. Ferreira[b,2], Mauro M. Teixeira[i], and Marcello Allegretti[a,2]

[a]Department of Discovery, Dompé SpA Research Center, 67100 L'Aquila, Italy; [b]Department of Pharmacology, Ribeirao Preto Medical School, University of Sao Paulo, 14049-900, Ribeirao Preto, Brazil; [c]Dipartimento di Farmacia, Viale Area delle Scienze 27/A, Università degli Studi di Parma, 43121 Parma, Italy; [d]ALTA Ricerca e Sviluppo in Biotecnologie S.r.l.u, 67100 L'Aquila, Italy; [e]Department of Biomedical, Surgical and Dental Sciences, University of Milan, I-20133 Milan, Italy; [f]Istituto di Ricerca e Cura a Carattere Scientifico (IRCCS) Galeazzi Orthopaedic Institute, I-20161 Milan, Italy; [g]Department of Medical Biotecnologies and Translational Medicine, University of Milan, I-20129 Milan, Italy; [h]Humanitas Clinical and Research Center, Rozzano, 20089 Milan, Italy; and [i]Imunofarmacologia, Departamento de Bioquímica e Immunologia, Instituto de Ciências Biológicas, Universidade Federal de Minas Gerais, 31270-901, Belo Horizonte, Brazil

www.pnas.org/cgi/doi/10.1073/pnas.1422166112

NEUROSCIENCE

Correction for "Individual differences in the peripheral immune system promote resilience versus susceptibility to social stress," by Georgia E. Hodes, Madeline L. Pfau, Marylene Leboeuf, Sam A. Golden, Daniel J. Christoffel, Dana Bregman, Nicole Rebusi, Mitra Heshmati, Hossein Aleyasin, Brandon L. Warren, Benoit Lebonté, Sarah Horn, Kyle A. Lapidus, Viktoria Stelzhammer, Erik H. F. Wong, Sabine Bahn, Vaishnav Krishnan, Carlos A. Bolaños-Guzman, James W. Murrough, Miriam Merad, and Scott J. Russo, which appeared in issue 45, November 11, 2014 of *Proc Natl Acad Sci* USA (111:16136–16141; first published October 20, 2014; 10.1073/pnas.1415191111).

The authors note that the author name Benoit Lebonté should instead appear as Benoit Labonté. The corrected author line appears below. The online version has been corrected.

Georgia E. Hodes, Madeline L. Pfau, Marylene Leboeuf, Sam A. Golden, Daniel J. Christoffel, Dana Bregman, Nicole Rebusi, Mitra Heshmati, Hossein Aleyasin, Brandon L. Warren, Benoit Labonté, Sarah Horn, Kyle A. Lapidus, Viktoria Stelzhammer, Erik H. F. Wong, Sabine Bahn, Vaishnav Krishnan, Carlos A. Bolaños-Guzman, James W. Murrough, Miriam Merad, and Scott J. Russo

www.pnas.org/cgi/doi/10.1073/pnas.1423575112

APPLIED PHYSICAL SCIENCES

Correction for "Motionless phase stepping in X-ray phase contrast imaging with a compact source," by Houxun Miao, Lei Chen, Eric E. Bennett, Nick M. Adamo, Andrew A. Gomella, Alexa M. DeLuca, Ajay Patel, Nicole Y. Morgan, and Han Wen, which appeared in issue 48, November 26, 2013, of *Proc Natl Acad Sci USA* (110:19268–19272; first published November 11, 2013; 10.1073/pnas.1311053110).

The authors note that on page 19269, right column, fifth full paragraph, line 4, "200 ms" should instead appear as "200 μs."

www.pnas.org/cgi/doi/10.1073/pnas.1423579112

Targeting the minor pocket of C5aR for the rational design of an oral allosteric inhibitor for inflammatory and neuropathic pain relief

Alessio Moriconi[a,1], Thiago M. Cunha[b,1], Guilherme R. Souza[b], Alexandre H. Lopes[b], Fernando Q. Cunha[b], Victor L. Carneiro[b], Larissa G. Pinto[b], Laura Brandolini[a], Andrea Aramini[a], Cinzia Bizzarri[a], Gianluca Bianchini[a], Andrea R. Beccari[a], Marco Fanton[a], Agostino Bruno[c], Gabriele Costantino[c], Riccardo Bertini[d], Emanuela Galliera[e,f], Massimo Locati[g,h], Sérgio H. Ferreira[b,2], Mauro M. Teixeira[i], and Marcello Allegretti[a,2]

[a]Department of Discovery, Dompé SpA Research Center, 67100 L'Aquila, Italy; [b]Department of Pharmacology, Ribeirao Preto Medical School, University of Sao Paulo, 14049-900, Ribeirao Preto, Brazil; [c]Dipartimento di Farmacia, Viale Area delle Scienze 27/A, Università degli Studi di Parma, 43121 Parma, Italy; [d]ALTA Ricerca e Sviluppo in Biotecnologie S.r.l.u, 67100 L'Aquila, Italy; [e]Department of Biomedical, Surgical and Dental Sciences, University of Milan, I-20133 Milan, Italy; [f]Istituto di Ricerca e Cura a Carattere Scientifico (IRCCS) Galeazzi Orthopaedic Institute, I-20161 Milan, Italy; [g]Department of Medical Biotecnologies and Translational Medicine, University of Milan, I-20129 Milan, Italy; [h]Humanitas Clinical and Research Center, Rozzano, 20089 Milan, Italy; and [i]Imunofarmacologia, Departamento de Bioquímica e Immunologia, Instituto de Ciências Biológicas, Universidade Federal de Minas Gerais, 31270-901, Belo Horizonte, Brazil

Contributed by Sérgio Henrique Ferreira, September 18, 2014 (sent for review March 15, 2014)

Chronic pain resulting from inflammatory and neuropathic disorders causes considerable economic and social burden. Pharmacological therapies currently available for certain types of pain are only partially effective and may cause severe adverse side effects. The C5a anaphylatoxin acting on its cognate G protein-coupled receptor (GPCR), C5aR, is a potent pronociceptive mediator in several models of inflammatory and neuropathic pain. Although there has long been interest in the identification of C5aR inhibitors, their development has been complicated, as for many peptidomimetic drugs, mostly by poor drug-like properties. Herein, we report the de novo design of a potent and selective C5aR noncompetitive allosteric inhibitor, DF2593A, guided by the hypothesis that an allosteric site, the "minor pocket," previously characterized in CXC chemokine receptors-1 and -2, is functionally conserved in the GPCR class. In vitro, DF2593A potently inhibited C5a-induced migration of human and rodent neutrophils. In vivo, oral administration of DF2593A effectively reduced mechanical hyperalgesia in several models of acute and chronic inflammatory and neuropathic pain, without any apparent side effects. Mechanical hyperalgesia after spared nerve injury was also reduced in *C5aR*$^{-/-}$ mice compared with WT mice. Furthermore, treatment of C5aR$^{-/-}$ mice with DF2593A did not produce any further antinociceptive effect compared with C5aR$^{-/-}$ mice treated with vehicle. The successful medicinal chemistry strategy confirms that a conserved minor pocket is amenable for the rational design of selective inhibitors and the pharmacological results support that the allosteric blockade of the C5aR represents a highly promising therapeutic approach to control chronic inflammatory and neuropathic pain.

C5a | inflammatory pain | neuropathic pain | allosteric antagonism | GPCR

Inflammatory and neuropathic pain are the most prevalent types of pathological pain and represent important health problems. Whereas inflammatory pain is one of the classic symptoms of the inflammatory process, neuropathic pain arises from any of multiple nerve lesions or diseases, with symptoms including hyperalgesia or allodynia (1, 2). Some of the most powerful painkillers, including opioids and nonsteroidal anti-inflammatory drugs, are only partially effective and prolonged exposure can cause unwanted effects (3, 4). As a result, there is continuous effort to identify novel therapeutics for pain control with alternative biological mechanisms and that elicit fewer side effects.

Inflammatory mediators, including cytokines/chemokines, play a critical role in the pathogenesis of inflammatory and neuropathic pain (5, 6). Emerging evidences suggest that C5a, the anaphylatoxin produced by complement activation, has potent nociceptive activity in several models of inflammatory and neuropathic pain by interacting with its selective receptor C5aR (7, 8). C5aR belongs to the class A subfamily of the seven-transmembrane (TM) G protein-coupled receptors (GPCR) (9) and is widely expressed in immune cells, including neutrophils (polymorphonuclear cells, PMN), monocytes, microglia, and in nonimmune cells, including neurons in the CNS and dorsal root ganglia (10, 11).

Evidence for a role of C5a in nociception sensitization has been obtained in several models of inflammatory pain. For example, C5a was produced at the inflammatory sites and elicited mechanical hyperalgesia by activating the C5aR on infiltrated PMN (7). Direct intraplantar injection of C5a in mice elicited both heat and mechanical hyperalgesia by sensitizing primary afferent C-nociceptors (12, 13). Local activation of C5aR has been also implicated in the pathogenesis of postsurgical pain, a model of postoperative pain (13). Finally, local administration of PMX-53, a C5aR antagonist, attenuated mechanical hyperalgesia induced by carrageenan, zymosan, or lipopolysaccharide (7). In addition to the peripheral role of C5a/C5aR in inflammatory pain, up-regulated levels of C5 and C5aR have been

Significance

Persistent pain in inflammatory and neuropathic conditions is often refractory to conventional analgesic therapy, with most patients suffering with unrelieved pain and serious treatment-related side effects. There is still a tremendous need to identify novel therapeutics for pain control with innovative biological mechanisms and minimal side effects. In this paper we challenge the hypothesis that a conserved structural motif across the G protein-coupled receptor family plays a regulatory role in the negative modulation of receptor activation and use a multidisciplinary approach to the rational drug design and characterization of a novel potent allosteric inhibitor of the C5a anaphylatoxin receptor (C5aR), thus providing a new promising avenue for the improvement of pharmacotherapy of chronic pain.

Author contributions: A.M., T.M.C., F.Q.C., A.A., M.L., S.H.F., M.M.T., and M.A. designed research; T.M.C., G.R.S., A.H.L., V.L.C., L.G.P., L.B., C.B., G.B., A.R.B., M.F., A.B., G.C., R.B., and E.G. performed research; G.B. contributed new reagents/analytic tools; A.M., T.M.C., G.R.S., F.Q.C., L.B., A.A., C.B., R.B., E.G., M.L., and M.M.T. analyzed data; A.M., T.M.C., A.A., M.M.T., and M.A. wrote the paper; and A.R.B., M.F., A.B., and G.C. performed computational studies.

The authors declare no conflict of interest.

Freely available online through the PNAS open access option.

[1]A.M. and T.M.C. contributed equally to this work.

[2]To whom correspondence may be addressed. Email: shferrei@fmrp.usp.br or marcello.allegretti@dompe.it.

This article contains supporting information online at www.pnas.org/lookup/suppl/doi:10.1073/pnas.1417365111/-/DCSupplemental.

found in spinal cord microglia in animals subjected to spared nerve injury (SNI), a model of neuropathic pain (8). Indeed, C5-null mice or the infusion of PMX-53 into the intrathecal space reduced neuropathic pain hypersensitivity in the SNI model (8). Collectively, these data suggest that a neuroimmune interaction in the periphery and spinal cord through activation of the complement cascade and the production of C5a contributes to the genesis of both inflammatory and neuropathic pain.

As for other peptidergic GPCRs, the efforts to identify small molecular weight C5aR antagonists have led to a limited number of molecules, mostly lacking adequate potency and selectivity (14). The most promising candidate so far described, PMX-53, is a cyclic peptidomimetic antagonist designed to mimic the C-terminal portion of C5a (15). Despite the encouraging results obtained in preclinical studies, as for many peptide drugs, the development of PMX-53 has been limited by its short half-life and unfavorable bioavailability (16). In the present study, we report the successful design of a nonpeptidic C5a allosteric small molecular weight inhibitor driven by the structural information on a minor pocket spanning between TM1, -2, -3, -6, and -7 that is highly conserved across the GPCR family and that has been recently proposed as a key motif for the intracellular activation process. Reparixin was previously reported as a neutral allosteric inhibitor of CXCR1 and CXCR2 that binds the TM in a region that overlaps the minor pocket (17, 18). Combining the information from independent sources on structural and functional features of allosteric sites in homologous chemokine receptors, this paper intends to provide what is, to our knowledge, the first example of de novo design of a new class of allosteric small molecular weight inhibitors of a GPCR not belonging to the chemokine receptor family, C5aR. The preclinical candidate, DF2593A, is a potent and orally active C5a noncompetitive allosteric inhibitor with significant antinociceptive effects in a wide range of inflammatory and neuropathic pain models.

Results

Binding Mode Characterization of DF2593A to C5aR. The human C5aR (hC5aR) homology model was originally built using the human CXCR1-reparixin complex (19) as a template, and subsequently refined and compared with the C5aR model built starting from the human C–C chemokine receptor type 5 (hCCR5) crystal structure (PDB ID code 4MBS), in which CCR5 is bound with the marketed HIV allosteric drug maraviroc (20, 21). Sequence identity between hCCR5 and hC5aR is 21.3%, whereas sequence similarity is 52.4%. Despite a low sequence identity, the key structural features defining the minor pocket, the proline kink in TM2 and the water-mediated hydrogen bond network between the intracellular segments of TM1, -2, -3, -6, and -7, is highly conserved between chemokine receptors and C5aR. With the aim to develop a specific site-binding model in C5aR, the pattern of polar interactions involved in the anchorage of reparixin at CXCR1 was analyzed in detail (19). Two of the three key residues of TM3, -6, and -7 (Asn120$^{3.35}$, Tyr258$^{6.51}$, and Glu291$^{7.39}$) are fully conserved (Asn119$^{3.35}$ and Tyr258$^{6.51}$) in C5aR (19, 22), and the glutamic residue 7.39 (Val286$^{7.39}$ in C5aR) is replaced by Asp282$^{7.35}$ one helix turn above (Table S1). Furthermore, as for CXCR1, the minor pocket in C5aR is surrounded by a large cluster of hydrophobic residues (Leu41$^{1.36}$, Phe93$^{2.61}$, Ile96$^{2.64}$, and Leu278$^{7.31}$) in the upper region of the TM layer (Fig. 1*C*). Interestingly, Asp82$^{2.50}$, the crucial amino acid in the conserved motif of TM2:$L_{92\%}XXXD_{91\%}$ is also present in the binding cavity of C5aR (23). The formation of a hydrogen bond between Asp82$^{2.50}$ and Asn296$^{7.49}$ in TM7 is deemed crucial to activate C5aR (24). Accordingly, the freezing of Asp82$^{2.50}$ in the inactive position with DF2593A may prevent the crucial movement to switch C5aR to its active state and it may represent a mechanistic explanation for the inhibitory effect of DF2593A.

Based on these structural characteristics, a site-targeting library was designed to identify a new class of allosteric C5aR modulators. The phenylpropionic moiety was chosen as a privileged scaffold to accommodate the shallow crevice between TM2, -3, -6, and -7 and the trifluoromethyl group in the para position was selected as promising substituent to establish a bidentate interaction with Asn119$^{3.35}$ and Asp82$^{2.50}$ bridging TM3 and TM2 associated with the feature of the trifluoromethyl portion to engage additional hydrophobic interactions (25, 26) (Table S2, compound **1**). As we were seeking for the key polar interactions with Asp282$^{7.35}$ and Tyr258$^{6.51}$, a series of carboxamide and aminocarbonyl residues bearing basic groups were synthesized. We found flexible tertiary ω-aminoalkylamides (Table S2, compounds **2–3**) and dual significant inhibiting of C5a and CXCL8-induced chemotaxis, whereas the insertion of conformationally rigid cyclic structures led to a full selectivity versus the C5aR (Table S2, compounds **4–5**). The geometry and the electronic status of the amido group were previously demonstrated (25) to be key determinants to establish the polar network in CXCR1/2 binding sites. Thus, the simple inversion of the amide group in compound **2** was sufficient to loose affinity at CXCR1/2, leading to the fully C5aR-selective isomer **6**. The optimization of the alkyl chain length and hydrophobicity (Table S2, compounds **6–12**) led to the selection of DF2593A (Table S2, compound **9**) as the most promising lead for further in vitro and in vivo characterization (Fig. 1*A*). Extensive molecular dynamics and automatic docking runs on the C5aR/DF2593A complex were performed to generate a reliable binding mode hypothesis. Based on the refined model, DF2593A is able to bind C5aR by two principal polar interaction patterns: (*i*) charge–charge interaction between Asp282$^{7.35}$and the charged nitrogen of the piperidine ring of DF2593A, and (*ii*) a network of polar interactions between the triflate and the couple Asn119$^{3.35}$/Asp82$^{2.50}$. Intriguingly, halogen-bond interactions are engaged between fluorine atoms and carbonyl oxygen of both Asn119$^{3.35}$ and Asp82$^{2.50}$.

The polar network is reinforced by the hydrogen bond between the carbonyl group of Ile116$^{3.32}$ and the amide moiety of DF2593A. In addition, the phenyl ring of DF2593A is involved in a π–π interaction with Tyr290$^{7.43}$. As mentioned, the binding cavity is also surrounded by hydrophobic residues, like Leu41$^{1.36}$, Phe93$^{2.61}$, Ile96$^{2.64}$, Leu278$^{7.31}$, and Val286$^{7.39}$ (Fig. 1 *B* and *C*). It has been observed that the Val286Ala$^{7.39}$ mutant led to a moderately inactive C5aR, supporting the hypothesis of a prominent functional role of TM7 (27).

The allosteric nature of the C5aR minor pocket (17) and the inhibitory activity of DF2593A were then investigated. Wild-type receptor and seven Ala-scanning mutants of C5aR were transiently transfected in L1.2 cells and tested for functionality. All mutants but Asp282$^{7.35}$ were nonsignificantly impaired in their cell-surface expression (Fig. S1) and sustained effective cell migration in response to C5a (Fig. S2). Transfectants were then tested in the C5a-induced chemotaxis assay in presence of increasing concentrations of DF2593A. As shown in Fig. 1*D*, the Asn119$^{3.35}$Ala mutant is fully resistant to inhibition by DF2593A, supporting the hypothesis that Asn119$^{3.35}$ is a key residue for ligand recognition. The dramatic effect of Tyr258$^{6.51}$ Ala mutant was coherent with the ligand/receptor complex in which the interaction established by the phenol group is essential to orientate Asp282$^{7.35}$ toward the piperidine nitrogen of DF2593A. The Tyr258$^{6.51}$ hydroxyl group could also act as a hydrogen-bond donor versus the carbonyl group in the central amide moiety of DF2593A. According to the proposed model, also the bulky hydrophobic Leu41$^{1.36}$, Phe93$^{2.61}$, Ile96$^{2.64}$, and Leu278$^{7.31}$—even though not directly involved in ligand binding—are structural and energetic determinants of the hydrophobic domain governing the pattern of interactions within the hydrophobic cluster. The replacement of these residues with Ala profoundly alters the shape and size of the pocket and coherently significantly compromises DF2593A potency. Notably, sequence alignment confirmed that key residues involved in the putative DF2593A binding mode are well conserved in both rat and mouse orthologs, supporting the potential of the candidate for further preclinical pharmacology studies (Fig. S3).

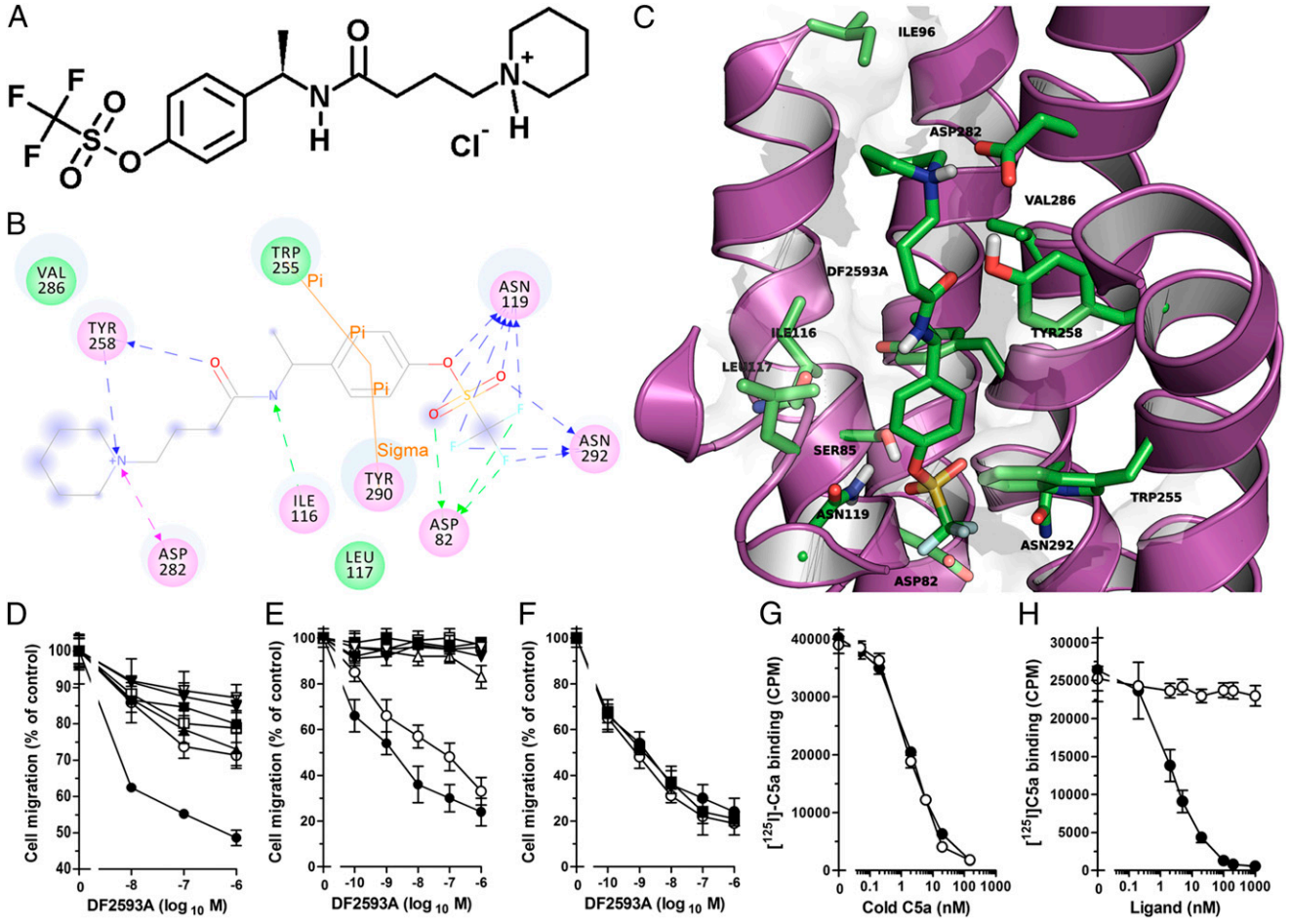

Fig. 1. DF2593A is a selective noncompetitive allosteric inhibitor of C5aR. (*A*) Two-dimensional structure of DF2593A. (*B*) Two-dimensional representation of DF2593A binding mode inside C5aR. Pink, green/blue and orange lines represent, respectively: charge–charge interaction, H-bond/halogen-bond interaction, π–π and σ interactions. (*C*) Three-dimensional representation of DF2593A in the TM region of C5aR (violet). Interacting residues are shown using the following color scheme: C (green), N (blue), O (red), S (yellow), F (cyan), and H (white); labeling is based on the Ballesteros–Weinstein numbering scheme. (*D*) Effect of DF2593A on the C5a-induced migration of WT (●), L41A (○), F93A (□), I96A (▲), L278A (▼), N119A (▽), and Y258A (■) C5aR/L1.2 transfectants pre-incubated with indicated DF2593A concentrations and then stimulated with 10 nM of C5a for 4 h. All mutants show a significant ($P < 0.05$) resistance to DF2593A at all doses tested compared with WT C5aR transfectants. (*E*) Effect of DF2593A on the C5a-induced migration of human PMN preincubated for 15 min with indicated DF2593A concentrations and then stimulated with 10 nM C5a (●), 1 μM C5a-desarg (○), 10 nM CXCL1 (□), 1 nM CXCL8 (▲), 10 nM CXCL12 (△), 30 nM CCL3 (▼), and 10 nM fMLP (▼) for 1 h. Significant inhibition was observed for C5a (at doses above 10^{-10} M) and C5a-desarg (at doses above 10^{-9} M). (*F*) Effect of DF2593A on the C5a-induced migration of human (■), mouse (○) and rat (●) PMN preincubated with indicated DF2593A concentrations and then stimulated with 10 nM C5a of corresponding origin. All leukocytes were significantly inhibited at doses above 10^{-10} M and were equally sensitive. (*G*) Human PMN incubation with vehicle (●) or 1 μM of DF2593A (○) and then aliquots of 0.2 nM of [^{125}I]-C5a and serial dilution of cold C5a were added to 10^6 cells in 100 mL of binding medium. There was no significant difference between vehicle and DF2593A. (*H*) Human PMN were directly exposed to vehicle or different concentrations of DF2593A (○) and then aliquots of 0.2 nM of [^{125}I]-C5a and vehicle (DF2593A-treated PMN) or serial dilution of unlabeled C5a (vehicle-treated PMN) (●) were added to 10^6 cells in 100 mL of binding medium. Significant difference were observed at doses above 10^{-9} M. In *D* to *F*, data are expressed as percent of migrated cells observed in the absence of DF2593A (mean ± SD of three independent experiments). $P < 0.01$ versus cell migration in the absence of DF2593A by Mann–Whitney *U* test. In *G* and *H*, data are reported as mean ± SD of three independent experiments.

In Vitro Characterization of DF2593A. Pharmacological characterization showed that DF2593A did not inhibit spontaneous cell migration per se and was >1,000-fold selective versus other chemoattractants, including CXCL8 and CXCL1 (IC_{50} > 10 μM) (Fig. 1*E*). DF2593A effectively inhibited C5a-induced human PMN migration (IC_{50} = 5.0 nM) and cross-reacted with rat and mouse orthologs (IC_{50} = 6.0 nM and IC_{50} = 1.0 nM, respectively) (Fig. 1*F*). DF2593A (tested at 10 μM) was selective on a panel of different GPCRs (Table S3) and ion channels (Table S4) and was also completely inactive (percent inhibition = 10 ± 3; mean ± SD; three experiments performed in duplicate) in a prostaglandin E_2 (PGE_2) production assay (28).

Binding experiments carried out on PMN membranes with radiolabeled C5a showed that DF2593A did not compete with binding of C5a. Pretreatment of PMN with DF2593A (1 μM) did not change C5a affinity for C5aR (K_d = 1.8 ± 1 nM and 1.0 ± 0.4 nM in vehicle and DF2593A-treated groups, respectively; $n = 3$ per group). In addition, DF2593A did not affect the number of C5aR molecules expressed on the cell membrane (127,000 ± 13,000 and 133,000 ± 21,000 binding sites per cell in vehicle and DF2593A-treated groups, respectively) and did not alter C5a binding to C5aR in displacement experiments (Fig. 1 *G* and *H*).

Pharmacokinetic Profile of DF2593A. The pharmacokinetics of DF2593A was investigated in mouse after intravenous and oral administration. Following oral administration (1 mg/kg) in mice, DF2593A was well absorbed (F = 83%) with a C_{max} of 0.1 μM, a t_{max} of 1.2 h, and plasma samples harvested over a period of 12 h generated free plasma drug concentrations in the range 0.016–0.004 μM, about 4- to 16-fold greater than its in vitro IC_{50}. For

brain permeation studies, DF2593A was dosed intravenously at 10 mg/kg and the levels of DF2593A were 913 ng/g tissue and 673 ng/mL in brain and plasma, respectively, at 5 min postdose. At 8 h postdose, significant levels of DF2593A were still present in the brain (114 ng/g) and also in the plasma (56 ng/mL). The brain-to-plasma ratios of DF2593A ranged from 1.36 (at 5 min postdose) to 2.04 at 8 h postdose. In parallel, the distribution coefficient, logBB, increased from 0.13 (at 5 min) to 0.3 (at 8 h), suggesting good permeation of the molecule into the brain.

Antinociceptive Effects of DF2593A in Several Models of Inflammatory Pain. C5a/C5aR interactions mediate carrageenan-induced mechanical hyperalgesia in rodents, suggesting it was a reasonable model to evaluate the potential analgesic effect of DF2593A (7). Corroborating this finding, carrageenan-induced inflammatory hyperalgesia is reduced in C5aR$^{-/-}$ mice compared with WT mice (Fig. S4). Consistent with its in vitro potency, oral administration of DF2593A inhibited carrageenan-induced mechanical hyperalgesia in a dose-dependent manner, but did not alter mechanical threshold in naive mice (Fig. 2*A*). C5a-induced hyperalgesia was also blocked by DF2593A, supporting the concept that DF2593A blocks hyperalgesia by inhibiting the C5aR (Fig. 2*B*). Neither DF2593A nor C5aR$^{-/-}$ deletion affected mechanical hyperalgesia induced by PGE_2 injected in the mice paws (Fig. 2*C* and Fig. S4). Furthermore, DF2593A did not alter epinephrine-induced hyperalgesia in the mice paws (Fig. 2*C*). In attempt to test the effect of DF2593A against chemical nociception, a writhing test induced by zymosan was studied (29). Oral treatment of mice with DF2593A significantly reduced zymosan-induced writhing response (Fig. 2*D*). DF2593A had no opioid-like affect in the hot-plate test and did not cause any motor impairment that could have accounted for the analgesic effects observed (Fig. 2 *E* and *F*). Treatment with DF2593A or genetic deletion of C5aR (C5aR$^{-/-}$ mice) did not alter carrageenan-induced PMN accumulation (Fig. S5), in agreement with our previous findings (7).

The analgesic effect of DF2593A was then tested in the complete Freund's adjuvant (CFA)-induced chronic inflammatory pain model. Oral pretreatment with DF2593A inhibited CFA-induced mechanical hyperalgesia (Fig. 3*A*). Consistent with its plasma levels, the effect of DF2593A was detected at least 6 h after CFA injection, but not at 24 h (Fig. 3*A*). Next, we probed whether the posttreatment with DF2593A could modify mechanical CFA-induced hyperalgesia and whether the analgesic effect was maintained. As reported in Fig. 3 *B* and *C*, delayed treatment with DF2593A (24 h after CFA injection) reduced CFA-induced mechanical and thermal inflammatory hyperalgesia. In a therapeutic setting, treatment with DF2593A starting at 24 h after CFA injection and then twice a day for 1 wk reduced mechanical hyperalgesia (Fig. 3*D*). Interestingly, the effect of DF2593A was maintained and when DF2593A treatment was stopped, mechanical hyperalgesia resumed to basal levels (Fig. 3*D*). There is evidence to suggest that C5a contributes to the pathogenesis of rheumatoid arthritis, including arthritic pain (7, 30). Therefore, in the next step we evaluated the effect of DF2593A in the genesis of articular hyperalgesia in two models of arthritis in mice, antigen- and zymosan-induced arthritis. Oral pretreatment with DF2593A effectively inhibited articular hyperalgesia in both models (Fig. 3 *E* and *F*).

Antinociceptive Effects of DF2593A in the SNI Model of Neuropathic Pain. Because activation of the complement system at the site of nerve injury and in the spinal cord contributes to induction and establishment of neuropathic pain (8, 31, 32), the effect of DF2593A in the SNI-induced neuropathic pain model in mice was evaluated. Oral treatment with DF2593A 7 d after surgery clearly reduced mechanical hypersensitivity induced by SNI (Fig. 4*A*). The effects of DF2593A persisted at least 6 h after treatment and, coherently with the pharmacokinetic profile, a progressive loss of antinociceptive effect was observed after 24 h (Fig. 4*A*). Confirming the involvement of C5aR in the genesis of neuropathic pain, mechanical hypersensitivity 7 d after SNI was also reduced in

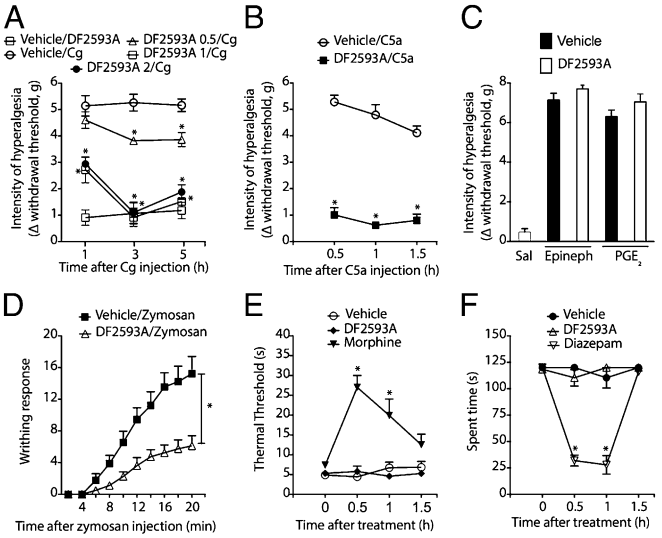

Fig. 2. Antinociceptive effects of DF2593A on acute inflammatory pain models. (*A*) Mice were treated orally with vehicle or DF2593A (0.5–2 mg/kg) 50 min before intraplantar injection of carrageenan (Cg, 100 μg per paw) or vehicle (saline). (*B*) Mice were treated orally with vehicle (saline) or DF2593A (1 mg/kg), 50 min before intraplantar injection of C5a (300 ng per paw). (*C*) Mice were treated orally with vehicle (saline) or DF2593A (1 mg/kg), 50 min before intraplantar injection of PGE_2 (100 ng per paw) or epinephrine (300 ng per paw). Mechanical hyperalgesia was evaluated 60 min after stimuli injection. (*D*) Mice were treated orally with vehicle (saline) or DF2593A (1 mg/kg) 50 min before intraperitoneal injection of zymosan (1 mg per cavity). The number of writhing responses induced by zymosan was evaluated for 20 min $n = 8$. (*E*) The thermal nociceptive threshold in naive mice was evaluated before and at indicated time after DF2593A treatment (1 mg/kg) using a hot-plate test. Morphine (8 mg/kg, s.c.) was used as a positive control. (*F*) Naive mice were treated orally with vehicle or DF2593A (1 mg/kg) followed at indicated times by evaluation in rota-rod test. Diazepam (7.5 mg/kg, s.c) was used as a positive control. Data are shown as mean ± SEM ($n = 6$–8 per group). *$P < 0.05$ compared with vehicle-treated animals.

C5aR$^{-/-}$ mice compared with WT mice (Fig. 4*B*). Furthermore, treatment of C5aR$^{-/-}$ mice with DF2593A did not produce any further antinociceptive effect compared with C5aR$^{-/-}$ mice treated with vehicle (Fig. 4*B*). The mechanical nociceptive threshold of C5aR$^{-/-}$ naive mice did not differ from WT mice (mechanical nociceptive threshold of naive WT mice: 7.2 ± 0.6 g and naive C5aR$^{-/-}$ mice: 6.8 ± 0.1 g).

In a therapeutic setting, DF2593A was given twice a day from day 7 to day 14 after surgery and mechanical hypersensitivity measured 6 h after the first daily dose. As seen in Fig. 4*C*, the effects of DF2593A were immediate and maintained over the observation period. Mechanical hypersensitivity returned to the same level of SNI control group 2 d after the suspension of the DF2593A treatment (Fig. 4*C*).

Discussion

This paper reports the molecular conception, synthesis, and characterization of the preclinical candidate DF2593A that shows potent and selective inhibitory effect on the C5a-induced PMN migration and optimal pharmacokinetic and pharmacological profile in a panel of relevant inflammatory and neuropathic pain experimental models.

In recent years, allosteric modulation of GPCRs has been proposed as a promising new paradigm for the design of potent and selective drugs with improved drug-like properties, finely modulating the receptor function. There is emerging evidence to suggest that, despite marked differences between the natural ligands, GPCRs share common activation mechanisms involving specific microswitches that regulate interhelical movements, which offer unprecedented opportunities for the rational drug design of

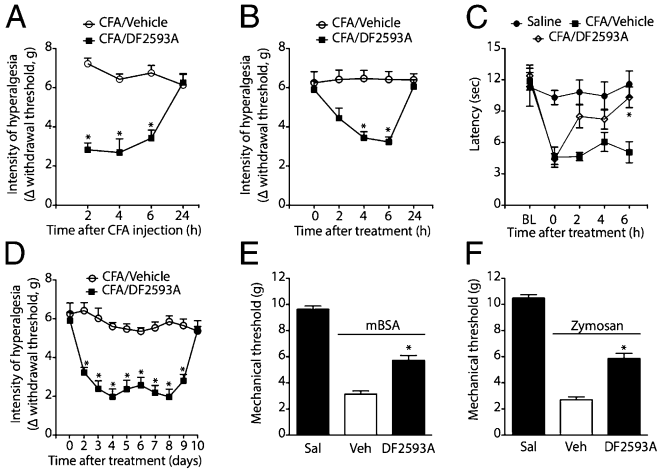

Fig. 3. Effects of DF2593A on CFA-induced mechanical and thermal hyperalgesia and arthritic nociception. (*A*) Mice were treated orally with vehicle or DF2593A (1 mg/kg) 50 min before intraplantar injection of CFA (10 μL per paw). (*B*) Mice were treated orally with vehicle or DF2593A (1 mg/kg) 24 h after intraplantar injection of CFA (10 μL per paw). Mechanical or (*C*) thermal nociceptive threshold was evaluated 2–24 h after DF2593A treatment. (*D*) DF2593A (1 mg/kg) or vehicle was given at 24 h after CFA injection and then twice a day until 7 d after CFA. Mechanical hyperalgesia was evaluated at 6 h after the first daily dose of DF2593A. (*E* and *F*) Mice were pretreated orally with vehicle (saline) or DF2593A (1 mg/kg) 50 min before intra-articular injection of mBSA (30 μg per joint) in immunized mice or before intra-articular injection of zymosan (150 μg per joint) in naive mice. Mechanical nociceptive threshold was evaluated 6 h after stimuli injection. Data are shown as mean ± SEM ($n = 6$ per group). $^*P < 0.05$ compared with vehicle-treated animals.

novel allosteric modulators. In this context, modeling and crystallographic studies of the GPCRs have identified in the TM region of GPCRs, a major pocket and a minor pocket, which has been proposed as a "triggering domain" not involved in natural ligand binding but crucial for the fine tuning of the global receptor activation process (17). Previous studies elucidated that reparixin, an allosteric inhibitor of CXCL8 receptors, binds CXCR1 within the minor pocket, locking the receptor in the inactive state by interhelical polar interactions with residues of TM1, -3, -6, and -7 (19).

Guided by the hypothesis that this minor pocket may represent a functionally conserved site across the GPCR family, homology modeling studies and molecular dynamics simulations of C5aR were carried out. Despite the low overall identity between C5aR and chemokine receptors, sequence analysis revealed that the three key residues identified for reparixin and CXCR1 are conserved in C5aR (22). Taking advantage of the structural diversity of other residues surrounding the minor pocket in C5aR and CXCR1, rational design was addressed by targeting a specific pattern of interactions to retain full selectivity to C5aR. Extensive site-directed mutagenesis studies in C5aR confirmed that this region is not directly involved in ligand receptor binding or critical for receptor activation and function. This finding nicely fits with the most accredited model of C5a/C5aR interaction (33), according to which the flexible C-terminal of C5a is implicated in the recognition of a domain distinct from the allosteric pocket and delimited mainly by $Arg206^{5.42}$, TM4, and the second extracellular loop. Nevertheless, our studies clearly demonstrated that specific ligands at this minor but conserved site are potent inhibitors of the C5a-induced chemotaxis, acting as neutral noncompetitive allosteric inhibitors. Interestingly, as the key residues involved are well conserved in both rat and mouse orthologs, the above results pave the way for the rational design of allosteric C5aR inhibitors with most favorable cross-species reactivity characteristics.

Previous studies have characterized the role of the C5a/C5aR signaling in the genesis of inflammatory and neuropathic pain (7, 8). Neuropathic pain is an important and relatively common clinical condition and available therapies are only partially effective. Among the events implicated in the genesis of neuropathic pain, neuroimmune interactions, including spinal activation of glial cells and the production of proinflammatory mediators, seem to be important for pain amplification. It was shown that expression of common genes, including the complement system genes, occurred in three different models of peripheral neuropathy (8). These findings are in agreement with the inhibition of complement activation by the intrathecal administration of a soluble human complement receptor type 1, which prevented the activation of C3 and C5 convertases and reduced mechanical allodynia in various neuropathic pain models (31). Additionally, C6-deficient rats still presented nerve injury-induced mechanical allodynia, suggesting that the membrane attack complex assembling is not necessary for the induction of neuropathic pain states (8). Accordingly, the nociceptive activity of the complement system appears to be strongly dependent on the C5a/C5aR interaction. Indeed, after nerve injury, expression of C5aR and C5 in the microglial cells of the spinal cord increased, and C5-deficient mice or intrathecal treatment with the classic antagonist PMX-53 ameliorated nerve injury-induced allodynia (8). Taken together, this preclinical evidence strongly supports the hypothesis that C5aR is an interesting target for neuropathic pain control.

The precise cellular site of action of DF2593A in the nociceptive system is not fully understood. Considering the aforementioned evidence of a role of C5a in the CNS, the efficacy of DF2593A in the SNI model may arise in part from its permeability to the blood–brain barrier. However, activation of the complement system in the periphery, at the level of nerve injury and dorsal root ganglia, could also contribute to the genesis of neuropathic pain (32, 34). In the periphery, DF2593A could disrupt the activation and the recruitment of leukocytes, thus attenuating the direct sensitization of the primary nociceptive neurons expressing C5aR (35). Importantly, DF2593A was effective even when given 1 wk after SNI, and nociceptive hypersensitivity returned to basal values when the DF2593A treatment was halted. These results clearly confirm the therapeutic potential of DF2593A and show that continuous activation of the C5aR is relevant for induction and maintenance of nociceptive hypersensitivity in the SNI model.

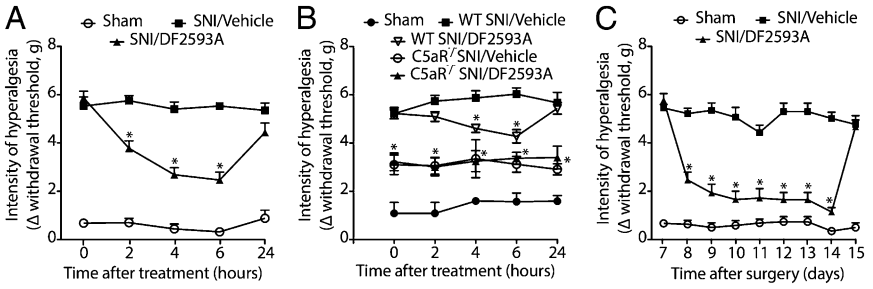

Fig. 4. Antinociceptive effects of DF2593A in the SNI model of neuropathic pain. (*A*) DF2593A (1 mg/kg) or vehicle (saline) were given orally 7 d after SNI surgery in mice. Mechanical hypersensitivity was evaluated from 2 to 24 h after oral administration of DF2593A. (*B*) Mechanical hypersensitivity was evaluated 7 d after SNI surgery in WT and $C5aR^{-/-}$ mice (time 0), followed by the treatment with vehicle or DF2593A (1 mg/kg). Mechanical hypersensitivity was then evaluated 2–24 h after DF2593A or vehicle treatment. (*C*) DF2593A (1 mg/kg per dose) or vehicle (saline) were given at day 7 and then twice a day until 14 d after SNI. Mechanical hypersensitivity was evaluated at 6 h after the first daily dose of DF2593A during 1 wk. Data are shown as mean ± SEM ($n = 6$ per group). $^*P < 0.05$ compared with vehicle-treated animals.

In the inflammatory pain models, the actions of C5a appeared to be sequential to PMN activation and are recruited into the inflammatory site in response to chemokines and lipid mediators (7). Recent evidence showed that C5aR is expressed in primary nociceptive neurons and that C5a could directly sensitize these fibers (12, 13). Our studies showed that DF2593A blocked carrageenan and C5a-dependent mechanical hyperalgesia in vivo without sedative or central opioid-like effects. Interestingly, DF2593A was also effective in a model of chronic inflammatory pain and in two models of inflammatory arthritic disease, even when administered 24 h after the induction of inflammation, sustaining the therapeutic potential of DF2593A and suggesting that C5a is continuously produced and participates in the events leading to maintenance of chronic inflammatory pain. On the other hand, DF2593A did not affect mechanical hyperalgesia induced by PGE_2 or epinephrine, which directly cause sensitization of primary nociceptive neurons (6). Therefore, the analgesic effects of DF2593A cannot be ascribed to a nonspecific action and is related to its ability to block C5a/C5aR signaling, presumably on both PMN and nociceptive neurons. Finally, it is important to point out that the results obtained with $C5aR^{-/-}$ mice strongly provide target validation/specificity for the effects of DF2593A.

Our findings underline the functional relevance of the minor pocket in GPCR that, although not directly involved in natural ligand binding, cooperates with the fine-tuning of the receptor activation process and represents an attractive structural determinant for rational design of innovative therapeutic compounds. Our pharmacological results not only provide further support to the role of C5a/C5aR signaling in the generation and maintenance of neuropathic pain, but also demonstrate that DF2593A represents an innovative noncompetitive allosteric drug candidate to control pain in multiple therapeutic indications.

Materials and Methods

See *SI Materials and Methods* for a full discussion of methods used.

Molecular Modeling. The TM domains of CXCR1, CXCR2, and C5aR were identified by sequence alignments with rhodopsin structure by using the MUSCLE software. The C5aR model was refined and compared with CCR5 (PDB ID code 4MBS) and further optimized by verifying the GPCR TM-fingerprints alignment (20, 21). The C5aR TM bundle was assembled and refined as described in *SI Materials and Methods* and the final C5aR structure was used to dock DF2593A using LiGen.

Cells and Migration Assay. PMN and L1.2 cells migration was evaluated using a 48-well microchemotaxis chamber, as previously described (19).

Mechanical Nociceptive Paw Test in Mice. Mechanical hyperalgesia was tested in C57BL/6, BALB/C mice and in C5aR-deficient mice ($C5aR^{-/-}$) using the electronic von Frey test, as previously reported (6).

SNI-Induced Neuropathic Pain-Like Behavior. The SNI procedure comprised an axotomy and ligation of the tibial and common peroneal nerves, leaving the sural nerve intact (36).

Data Analyses and Statistics. For in vivo experiments, results are presented as mean ± SEM. The differences among the groups were compared by ANOVA (one-way) followed by Bonferroni's post hoc test. The level of significance was set at $P < 0.05$.

ACKNOWLEDGMENTS. The authors thank the technical assistance of Sergio Rosa and Ieda Schivo. This research was funded in part by the European Union Seventh Framework Programme (FP7-2007-2013) under Grant HEALTH-F4-2011-281608 (TIMER) and Grants 2011/19670-0 and 2013/08216-2 (Center for Research in Inflammatory Disease) from São Paulo Research Foundation (FAPESP).

1. Kidd BL, Urban LA (2001) Mechanisms of inflammatory pain. *Br J Anaesth* 87(1):3–11.
2. Baron R, Binder A, Wasner G (2010) Neuropathic pain: Diagnosis, pathophysiological mechanisms, and treatment. *Lancet Neurol* 9(8):807–819.
3. Schaffer D, et al. (2006) Risk of serious NSAID-related gastrointestinal events during long-term exposure: A systematic review. *Med J Aust* 185(9):501–506.
4. Devulder J, Jacobs A, Richarz U, Wiggett H (2009) Impact of opioid rescue medication for breakthrough pain on the efficacy and tolerability of long-acting opioids in patients with chronic non-malignant pain. *Br J Anaesth* 103(4):576–585.
5. White FA, Jung H, Miller RJ (2007) Chemokines and the pathophysiology of neuropathic pain. *Proc Natl Acad Sci USA* 104(51):20151–20158.
6. Cunha TM, et al. (2005) A cascade of cytokines mediates mechanical inflammatory hypernociception in mice. *Proc Natl Acad Sci USA* 102(5):1755–1760.
7. Ting E, et al. (2008) Role of complement C5a in mechanical inflammatory hypernociception: Potential use of C5a receptor antagonists to control inflammatory pain. *Br J Pharmacol* 153(5):1043–1053.
8. Griffin RS, et al. (2007) Complement induction in spinal cord microglia results in anaphylatoxin C5a-mediated pain hypersensitivity. *J Neurosci* 27(32):8699–8708.
9. Gerard C, Gerard NP (1994) C5A anaphylatoxin and its seven transmembrane-segment receptor. *Annu Rev Immunol* 12:775–808.
10. Zwirner J, Fayyazi A, Götze O (1999) Expression of the anaphylatoxin C5a receptor in non-myeloid cells. *Mol Immunol* 36(13-14):877–884.
11. Woodruff TM, Nandakumar KS, Tedesco F (2011) Inhibiting the C5-C5a receptor axis. *Mol Immunol* 48(14):1631–1642.
12. Jang JH, et al. (2010) Nociceptive sensitization by complement C5a and C3a in mouse. *Pain* 148(2):343–352.
13. Liang DY, et al. (2012) The complement component C5a receptor mediates pain and inflammation in a postsurgical pain model. *Pain* 153(2):366–372.
14. Horuk R (2009) Chemokine receptor antagonists: Overcoming developmental hurdles. *Nat Rev Drug Discov* 8(1):23–33.
15. Finch AM, et al. (1999) Low-molecular-weight peptidic and cyclic antagonists of the receptor for the complement factor C5a. *J Med Chem* 42(11):1965–1974.
16. Ricklin D, Lambris JD (2007) Complement-targeted therapeutics. *Nat Biotechnol* 25(11):1265–1275.
17. Rosenkilde MM, Benned-Jensen T, Frimurer TM, Schwartz TW (2010) The minor binding pocket: A major player in 7TM receptor activation. *Trends Pharmacol Sci* 31(12):567–574.
18. Bertini R, et al. (2012) Receptor binding mode and pharmacological characterization of a potent and selective dual CXCR1/CXCR2 non-competitive allosteric inhibitor. *Br J Pharmacol* 165(2):436–454.
19. Bertini R, et al. (2004) Noncompetitive allosteric inhibitors of the inflammatory chemokine receptors CXCR1 and CXCR2: Prevention of reperfusion injury. *Proc Natl Acad Sci USA* 101(32):11791–11796.
20. Fredriksson R, Lagerström MC, Lundin LG, Schiöth HB (2003) The G-protein-coupled receptors in the human genome form five main families. Phylogenetic analysis, paralogon groups, and fingerprints. *Mol Pharmacol* 63(6):1256–1272.
21. Allegretti M, et al. (2005) Targeting C5a: Recent advances in drug discovery. *Curr Med Chem* 12(2):217–236.
22. Allegretti M, et al. (2008) Allosteric inhibitors of chemoattractant receptors: Opportunities and pitfalls. *Trends Pharmacol Sci* 29(6):280–286.
23. Monk PN, Pease JE, Marland G, Barker MD (1994) Mutation of aspartate 82 of the human C5a receptor abolishes the secretory response to human C5a in transfected rat basophilic leukemia cells. *Eur J Immunol* 24(11):2922–2925.
24. Nikiforovich GV, Baranski TJ (2012) Structural mechanisms of constitutive activation in the C5a receptors with mutations in the extracellular loops: Molecular modeling study. *Proteins* 80(1):71–80.
25. Moriconi A, et al. (2007) Design of noncompetitive interleukin-8 inhibitors acting on CXCR1 and CXCR2. *J Med Chem* 50(17):3984–4002.
26. Bissantz C, Kuhn B, Stahl M (2010) A medicinal chemist's guide to molecular interactions. *J Med Chem* 53(14):5061–5084.
27. Gerber BO, Meng EC, Dotsch V, Baranski TJ, Bourne HR (2001) An activation switch in the ligand binding pocket of the C5a receptor. *J Biol Chem* 276(5):3394–3400.
28. Bizzarri C, et al. (2001) Selective inhibition of interleukin-8-induced neutrophil chemotaxis by ketoprofen isomers. *Biochem Pharmacol* 61(11):1429–1437.
29. Ribeiro RA, et al. (2000) Involvement of resident macrophages and mast cells in the writhing nociceptive response induced by zymosan and acetic acid in mice. *Eur J Pharmacol* 387(1):111–118.
30. Grant EP, et al. (2002) Essential role for the C5a receptor in regulating the effector phase of synovial infiltration and joint destruction in experimental arthritis. *J Exp Med* 196(11):1461–1471.
31. Twining CM, et al. (2005) Activation of the spinal cord complement cascade might contribute to mechanical allodynia induced by three animal models of spinal sensitization. *J Pain* 6(3):174–183.
32. Li M, Peake PW, Charlesworth JA, Tracey DJ, Moalem-Taylor G (2007) Complement activation contributes to leukocyte recruitment and neuropathic pain following peripheral nerve injury in rats. *Eur J Neurosci* 26(12):3486–3500.
33. Nikiforovich GV, Marshall GR, Baranski TJ (2008) Modeling molecular mechanisms of binding of the anaphylatoxin C5a to the C5a receptor. *Biochemistry* 47(10):3117–3130.
34. Levin ME, et al. (2008) Complement activation in the peripheral nervous system following the spinal nerve ligation model of neuropathic pain. *Pain* 137(1):182–201.
35. Levine JD, Gooding J, Donatoni P, Borden L, Goetzl EJ (1985) The role of the polymorphonuclear leukocyte in hyperalgesia. *J Neurosci* 5(11):3025–3029.
36. Decosterd I, Woolf CJ (2000) Spared nerve injury: An animal model of persistent peripheral neuropathic pain. *Pain* 87(2):149–158.

Supporting Information

Moriconi et al. 10.1073/pnas.1417365111

SI Materials and Methods

Reagents. Compounds were routinely dissolved at the indicated final concentrations in saline. All chemokines were from PeproTech. All chemicals, cell culture reagents, CFA, zymosan, C5a, and protease inhibitors were from Sigma. Dextran was from Pharmacia LKB. Diff-Quik was from Harleco. Boyden chambers and polycarbonate filter were from Neuroprobe. Transwell filters were from Costar. Thioglycolate and lipopolysaccharide (from *Escherichia coli* 055:B5) were from Difco. Pfx DNA polymerase and pcDNA3 were from Invitrogen. Human C5a monoclonal antibody was from BD PharMingen. Carrageenan was from FMC Corporation. [^{125}I]-C5a was from Amersham Pharmacia Biotech. For PGE_2 assay, the EIA kit (sensitivity 2.5 pg per well) was purchased by Amersham.

Migration Assay. The procedure for obtaining informed consent of the healthy donors from whom the peripheral blood was obtained included an oral explanation by the physician in charge of the investigation, or an authorized deputy, who illustrated the types of samples that would be withdrawn, the procedures that would be performed, the results that could be obtained, and their possible consequences for the donor. The donors then provided written informed consent approved by the S. Salvatore Hospital ethics committee. PMN were obtained from buffy-coat of heparinized human peripheral blood from adult healthy volunteers, as previously described (1). PMN were separated by dextran sedimentation (1) and murine PMN obtained by injection of 3% (vol/vol) thioglycollate into peritoneal cavities (1). Cell migration of PMN was evaluated using a 48-well microchemotaxis chamber, as previously described (1). Briefly, control medium (HBSS for human and rodent PMN) or chemoattractant solution (10 nM fMLP, 1 nM CXCL8, 10 nM CXCL1, 10 nM C5a, 10 nM CXCL12, 30 nM CCL3, 1 mM C5a des-Arg for hPMN, 10 nM mC5a or rC5a for murine PMN) were seeded in the lower compartment of the chamber and cell suspensions were seeded in the upper compartment. The migrated stained cells were counted by microscope. L1.2 migration was evaluated using 5-μ pore size Transwell filters, as previously described (2).

Generation of L1.2 Transfectants. C5aR cDNA coding sequence was cloned in the pcDNA3.1 expression vector and used to generate receptor mutants using the commercial Site-Directed Mutagenesis kit (Clontech). L1.2 cells were transiently transfected by electroporation as previously described (2). After 36 h from transfection, expression of C5a was assessed by flow cytometry using an anti-human C5a monoclonal antibody.

Radioligand Binding Assay. [^{125}I]-C5a (specific activity 2,200 Ci/mmol) binding on human PMN was performed as previously described (3). Nonspecific binding was determined by adding a 100-fold molar excess of unlabeled C5a. Scatchard analysis and all calculations were performed with the LIGAND program (4).

Macrophage Preparation and Lipopolysaccharide-Induced PGE_2 Production. Peritoneal exudates cells were collected as previously described (5). Briefly, mononuclear cells were split into 96 wells, preincubated with DF2593A, and then stimulated with lipopolysaccharide. The surnatants were harvested after 18 h and PGE_2 production was measured with an EIA kit.

Sequence Alignments and Molecular Modeling. All calculations were performed using Dell PowerEdge R815 Rack Server 4 sockets/24 cores, 128GB RAM, under the Microsoft Windows Server 2008 R2 operating system. CXCR1, CXCR2, and C5aR sequence alignments were obtained using the MUSCLE software (6) (Table S1). Human, mouse and rat C5aR sequences were aligned using MUSCLE software (Fig. S1). The C5aR homology model was built using CCR5 crystal structure (PDB ID code 4MBS) as a template, which is in bound-conformation with a small-molecule ligand (7, 8). Sequence identity between CCR5 and C5aR is 21.3%, and sequence similarity (BLOSUM65) is 52.4%. CXCR1/2 vs. C5aR sequences identity and similarity are, respectively, of 21.4% and 40.5% for CXCR1 and 26.2% and 49.9% for CXCR2. CCR5/C5AR sequence alignment was manually adjusted to ensure GPCRs TM-FPs alignment. The C5aR model was assembled and submitted to energy minimization cycles to reduce intra- and interhelical bumps between the amino acids side chains, by using the CHARMm force field with Momany–Rone partial charges in Discovery Studio 4.0 (Accelrys). The minimized model was submitted to MD runs (e = 1r) and heated to 300 K (heating time was 20 ps, equilibration time was 100 ps) with a production time of 1 ns (harmonic constrains were applied to the backbone to allow relaxations to C5aR without loose the secondary structure). After the MD, the last 100 ps of the run time were used to build an average structure of C5aR. DF2593A was docked in the allosteric binding cavity of C5aR for determining possible favorable ligand poses, by using the LiGenDock (9, 10) docking program. The final poses were clustered according to position and conformation, energy ranked, and visually inspected. The best-ranked poses were refined by in situ ligand minimization using Discovery Studio 4.0 with CHARMm forcefield and flexible binding-site residue treatment.

Compound Synthesis. All reagents and solvents for the synthesis of compounds **1**–**12** were purchased from Sigma-Aldrich or Lancaster and used without further purification. Optical rotations for compounds **1**–**12** were measured on a Perkin-Elmer 241 polarimeter and the $[\alpha]_D^{25}$ values are given in 10^{-1} deg·cm^2·g^{-1}. ^{1}H-NMR spectra were recorded on a Bruker AVANCE III 400 MHz spectrometer. Melting points were determined using a Büchi capillary melting point apparatus and are uncorrected. Reaction courses and product mixtures were monitored by TLC on silica gel (precoated F_{254} Macherey-Nagel plates); the spots were examined with UV light and visualized with I_2. The synthesis of compounds **1–3** (Table S2) was previously described (11, 12).

***Compound 4**: 4-{(2R)-1-[(1-methylpiperidin-4-yl)amino]-1-oxopropan-2-yl} phenyl trifluoromethanesulfonate.* To a solution of 4-phenyl trifluoromethanesulfonate acyl chloride derivatives (3.0 mmol) in CH_2Cl_2 (5 mL) and triethylamine (3.5 mmol) (prepared as described in ref. 8), 1-methylpiperidin-4-amine (3.0 mmol) was added portion-wise. The resulting solution was stirred for 3 h. After the disappearance of the starting material, triethylamonium chloride salt was filtered off and the solution was diluted with a saturated solution of $NaHCO_3$ (10 mL) and extracts with CH_2Cl_2 (3 × 10 mL). The collected organic extracts were dried over Na_2SO_4, filtered, and evaporated under vacuum to afford a crude 4-{(2R)-1-[(1-methylpiperidin-4-yl)amino]-1-oxopropan-2-yl}phenyl trifluoromethanesulfonate. The crude was purified by flash chromatography ($CHCl_3$/CH_3OH/cyclohexane/NH_4OH 60:14:24:2) to afford 4-{(2R)-1-[(1-methylpiperidin-4-yl)amino]-1-oxopropan-2-yl}phenyl trifluoromethanesulfonate (75% yield) as pale yellow oil. $[\alpha]_D^{25}$ (c = 0.3, CH_3OH): +40.3; ^{1}H-NMR (DMSO-d_6) δ 7.40 (d, 2H, J = 7 Hz), 7.25 (d, 2H, J = 7 Hz), 5.20 (bs, 1H, NH), 4.90 (q, 1H, J = 7Hz), 4.30 (m, 1H), 2.95(m, 2Hax), 2.30 (s, 3H), 2.12(m, 2Heq), 1.80(m, 4H), 1.45 (d, 3H, J = 7 Hz).

***Compound 5**: 4-{(2R)-1-[(8-methyl-8-azabicyclo[3.2.1]octan-3-amine]-1-oxopropan-2-yl}phenyl trifluoromethanesulfonate.* To a solution of 4-phenyl trifluoromethanesulfonate acyl chloride derivatives (3.0 mmol) in CH_2Cl_2 (5 mL) and triethylamine (3.5 mmol) (prepared as described in ref. 10), 8-methyl-8-azabicyclo[3.2.1]octan-3-amine (3.0 mmol) was added portion-wise, the resulting solution was stirred for 3 h. After the disappearance of the starting material, triethylamonium chloride salt was filtered off and the solution was diluted with a saturated solution of $NaHCO_3$ (10 mL) and extracts with CH_2Cl_2 (3 × 10 mL). The collected organic extracts were dried over Na_2SO_4, filtered, and evaporated under vacuum to afford a crude 4-{(2R)-1-[(8-methyl-8-azabicyclo[3.2.1]octan-3-amine]-1-oxopropan-2-yl}phenyl trifluoromethanesulfonate. The crude was purified by flash chromatography ($CHCl_3$/CH_3OH/cyclohexane/NH_4OH 60:14:24:2) to afford 4-{(2R)-1-[(8-methyl-8-azabicyclo[3.2.1]octan-3-amine]-1-oxopropan-2-yl}phenyl trifluoromethanesulfonate, (68% yield) as yellow oil.$[\alpha]_D^{25}$ (c = 0.3, CH_3OH): +29.3; ^{1}H-NMR (DMSO-d_6) δ 7.48 (d, 2H, J = 7 Hz), 7.25 (d, 2H, J = 7 Hz), 6.80 (bs, 1H, NH), 4.30 (m, 1H), 3.75 (m, 2Hax), 3.65 (q, 1H, J = 7 Hz), 2.75 (s, 3H), 2.60–1.90 (m, 8H), 1.45 (d, 3H, J = 7 Hz).

***Compound 6**: [4-[(1R)-1-(4-pyrrolidin-1-ylbutanoylamino)ethyl]phenyl] trifluoromethanesulfonate.* To a solution of ethyl 4-chlorobutyrate (0.465 mL, 3.32 mmol) in DMF (2 mL), pyrrolidine (0.831 mL, 9.96 mmol), triethylamine (1.4 mL, 9.96 mmol), and a catalytic amount of KI were added and the resulting solution was refluxed overnight. After cooling at room temperature, the solution was diluted with a saturated solution of $NaHCO_3$ (10 mL) and extracts with Et_2O (3 × 10 mL). The collected organic extracts were dried over Na_2SO_4, filtered, and evaporated under vacuum to give the ethyl 4-pyrrol-1-ylbutanoate as an oil (3 mmol), which was used without further purification. To a solution of the ester in dioxane (5 mL), few drops of 37% HCl were added and the solution was refluxed overnight. After cooling at room temperature, the solvent was evaporated under vacuum and the residue was dried overnight in oven at 60 °C in vacuo. The crude 4-pyrrolidin-1-ylbutanoic acid was dissolved in CH_3OH (4 mL) and $NaHCO_3$ (3 mmol) was added. After stirring for 2 h, the precipitate was filtered off and the mother liquors concentrated to afford the intermediate sodium 4-pyrrolidin-1-ylbutanoic acid (55% yield) as a colorless oil.^{1}H-NMR (DMSO-d_6) d3.35 (m, 2H), 2.80 (m, 2H), 2.70 (m, 2H), 2.15 (m, 4H), 1.75 (m, 4H). To a solution of sodium 4-pyrrolidin-1-ylbutanoic acid (0.381 g, 2.13 mmol) in dry CH_2Cl_2 (10 mL), 1,1′-carbonyldiimidazole (0.645 g, 2.13 mmol) was added and the resulting solution was left stirring at room temperature for 1 h. Triethylamine (0.597 mL, 4.25 mmol) and (1R)-1-[(4-trifluoromethanesulfonyloxy)phenyl] ethylamine hydrochloride (0.65 g, 2.13 mmol) were added and the resulting solution was left stirring at room temperature overnight. A saturated solution of $NaHCO_3$ (10 mL) was added and the two phases separated. The organic one was washed with extracts with a saturated solution of $NaHCO_3$ (2 × 5 mL), dried over Na_2SO_4, filtered, and evaporated under vacuum to give an oily residue. The crude was purified by flash chromatography ($CHCl_3$/CH_3OH/cyclohexane/NH_4OH 60:14:24:2) to afford [4-[(1R)-1-(4-pyrrolidin-1-ylbutanoylamino)ethyl]phenyl] trifluoromethanesulfonate (75% yield) as pale yellow oil. $[\alpha]_D^{25}$ (c = 0.3, CH_3OH): +40.3; ^{1}H-NMR (DMSO-d_6) δ 8.15 (bs, 1H, NH), 7.35 (q, 4H, J = 7 Hz), 4.90 (q, 1H, J = 7 Hz), 3.35 (m, 2H), 2.90 (m, 2H), 2.80 (m, 3H), 2.25 (t, 2H, J = 3 Hz), 1.95 (m, 4H), 1.75 (m, 4H).

***Compound 7**: [4-[(1R)-1-(3-pyrrolidin-1-ylpropanoylamino)ethyl]phenyl] trifluoromethanesulfonate.* Following the same procedure described for compound **6** and starting from pyrrolidine (0.325 mL, 3.9 mmol) and ethyl 3-chloropropanoate (0.177 mL, 1.3 mmol), sodium 3-(pyrrolidin-1-yl)propanoate was obtained as a pale yellow solid (62% yield).^{1}H-NMR (DMSO-d_6) d 3.35 (m, 2H), 2.80 (m, 2H), 2.70 (m, 4H), 1.75 (m, 4H). Compound **7** was then synthesized following the procedure described for compound **6** and starting from sodium 3-(pyrrolidin-1-yl)propanoate (0.231 g, 1.4 mmol) and (1R)-1-[(4-trifluoromethanesulfonyloxy)phenyl]ethylamine hydrochloride (0.458 g, 1.5 mmol) after workup and purification by flash chromatography ($CHCl_3$/CH_3OH/cyclohexane/NH_4OH 60:14:24:2). The title compound was obtained as yellow oil (55% yield). $[\alpha]_D^{25}$ (c = 0.3, CH_3OH): +52.3; ^{1}H-NMR (DMSO-d_6) δ 8.25 (bs, 1H, NH), 7.45 (q, 4H, J = 7 Hz), 5.01 (q, 1H, J = 7 Hz), 2.95 (m, 2H), 2.80 (m, 4H), 2.60 (m, 2H), 1.95 (m, 4H), 1.45 (d, 3H, J = 7 Hz).

***Compound 8**: [4-[(1R)-1-[3-(1-piperidyl)propanoylamino]ethyl]phenyl] trifluoromethanesulfonate.* According the same procedure described for compound **6** and starting from piperidine (0.385 mL, 3.9 mmol) and ethyl 3-chloropropanoate (0.177 mL, 1.3 mmol), sodium 3-(1-piperidyl)propanoic acid was obtained as a pale yellow solid (78% yield).^{1}H-NMR (DMSO-d_6) d 3.35 (m, 2H), 2.80 (m, 2H), 2.15 (m, 2H), 1.95 (m, 2H), 1.75 (m, 6H). Compound **8** was then synthesized following the same procedure described for compound **6** and starting from (1R)-1-[(4-trifluoromethanesulfonyloxy)phenyl]ethylamine hydrochloride (0.335 g, 1.1 mmol) and sodium 3-(1-piperidyl)propanoic acid (0.200 g, 1.12 mmol) to afford [4-[(1R)-1-[3-(1-piperidyl)propanoylamino]ethyl]phenyl] trifluoromethanesulfonateas yellow oil (63% yield). $[\alpha]_D^{25}$ (c = 0.1, CH_3OH): +48; ^{1}H-NMR ($CDCl_3$) δ 7.60 (bs, 1H, NH), 7.40 (d, 2H, J = 7 Hz), 7.25 (d, 2H, J = 7 Hz), 5.15 (q, 1H, J = 7 Hz), 2.95 (m, 2H), 2.55 (m, 4H), 2.35 (t, 2H, J = 3 Hz), 1.85–1.70 (m, 6H), 1.45 (d, 3H, J = 7 Hz).

***Compound 9**: N-[(1R)-1-(4-trifluoromethanesulfonyloxy)phenylethyl]-4-piperidin-1-ylbutanamide.* According the same procedure described for compound **6** and starting from piperidine (0.385 mL, 3.9 mmol) and ethyl 4-chlorobutyrate (0.182 mL, 1.3 mmol), sodium 4-(piperidin-1-yl)butanoate was obtained as a white solid (76% yield). ^{1}H-NMR (DMSO-d_6) d 3.35 (m, 2H), 2.80 (m, 2H), 2.70 (m, 2H), 2.15 (t, 2H, J = 3 Hz), 1.95 (m, 2H), 1.75 (m, 6H). Compound **9** was then obtained following the same procedure described for compound **6** and starting from (1R)-1-[(4-trifluoromethanesulfonyloxy)phenyl] ethylamine hydrochloride (0.305 g, 1 mmol) and sodium 4-(piperidin-1-yl)butanoate (0.193 g, 1 mmol). The crude was purified by flash chromatography ($CHCl_3$/CH_3OH/cyclohexane/NH_4OH 60:14:24:2) to afford *N*-[(1R)-1-(4-trifluoromethanesulfonyloxy)phenylethyl]-4-piperidin-1-ylbutanamide (75% yield) as pale yellow oil. $[\alpha]_D^{25}$ (c = 0.1, CH_3OH): +40; ^{1}H-NMR ($CDCl_3$) δ 7.60 (bs, 1H, NH), 7.40 (d, 2H, J = 7 Hz), 7.25 (d, 2H, J = 7 Hz), 5.15 (q, 1H, J = 7 Hz), 2.95 (m, 2H), 2.55 (m, 6H), 2.35 (t, 2H, J = 3 Hz), 1.85–1.70 (m, 6H), 1.45 (d, 3H, J = 7 Hz).

***Compound 10**: (2R)-2-(3-benzoylphenyl)-N-hydroxypropanamide.* In a 25-mL round-bottomed flask equipped with a magnetic stirrer, a solution of hydroxylamine hydrochloride (0.046 g, 0.66 mmol) and TEA (121 μL, 0.88 mmol) in $CHCl_3$ (2 mL) was stirred at room temperature for 15 min.

Separately, a solution of (*R*) - Ketoprofen (0.056 g, 0.22 mmol) in $SOCl_2$ (3 mL) was refluxed for 3 h. After cooling at room temperature, excess $SOCl_2$ was distilled off under vacuum and the crude acyl chloride diluted with $CHCl_3$ (5 mL) and slowly added into the hydroxylamine solution at T = 0 °C. After ice bath removal, the reaction mixture was stirred for additional 2.5 h, then was diluted in $CHCl_3$ (30 mL), washed with 10% $KHSO_4$ (3 × 10 mL), brine (3 × 10 mL), and dried over anhydrous Na_2SO_4 to give a crude that, after purification by flash chromatography ($CHCl_3$/CH_3OH 98:2), afforded pure (2R)-2-(3-benzoylphenyl)-N-hydroxypropanamide (0.040 g, 0.15 mmol) as a white waxy solid (68%). $[\alpha]_D^{25}$ (c = 0.34, CH_3OH): −28; ^{1}H-NMR ($CDCl_3$) δ 10.5 (bs, 1H, NH), 7.81–7.78 (m, 3H), 7.70–7.68 (m, 1H), 7.59–7.55 (m, 2H), 7.49–7.43 (m, 3H), 7.30 (bs, 1H, OH), 3.85 (q, 1H, J = 7 Hz), 1.45 (d, 3H, J = 7 Hz).

***Compound 11**: (2R)-2-[3-(furan-2-ylcarbonyl)phenyl]-N-[4-(trifluoromethyl)-1,3-thiazol-2-yl]propanamide.* To a solution of (*2R*)-2-[3-(furan-2-ylcarbonyl)phenyl]propanoic acid (0.078 g, 0.32 mmol) in dry CH_2Cl_2 (5 mL), CDI (0.055 g, 0.34 mmol) was added and the resulting

solution was stirred for 1 h at T = 0 °C. After ice-water bath removal 4-(trifluoromethyl)-1,3-thiazol-2-amine (0.057 g, 0.34 mmol) and TEA (40 μL, 0.29 mmol) were added and the resulting mixture was stirred at room temperature for 12 h. At the complete disappearance of the starting material, a buffer $H_3PO_4/H_2PO_4^-$ solution (pH = 2.0, 5 mL) was added and the reaction mixture was transferred into a separatory funnel. The two phases were separated and the organic one washed with the same buffer (3 × 5 mL), dried over Na_2SO_4, and evaporated under vacuum to give a crude, which was purified by flash chromatography ($CHCl_3/CH_3OH$ 95:5). Pure (2R)-2-[3-(furan-2-ylcarbonyl)phenyl]-N-[4-(trifluoromethyl)-1,3-thiazol-2 yl] propanamide (0.091 g, 0.23 mmol) was isolated as a pale brown solid (72%). $[\alpha]_D^{25}$ (c = 0.26, CH_3OH): −17.6; ^{1}H-NMR ($CDCl_3$) δ 8.90 (bs, 1H, NH), 8.00–7.90 (m, 2H), 7.70 (s, 1H), 7.59–7.55 (m, 2H), 7.4 (s, 1H), 7.30–7.10 (m, 1H), 6.60 (s, 1H), 3.90 (q, 1H, J = 7 Hz), 1.75 (d, 3H, J = 7 Hz).

***Compound 12**: [4-[(1R)-1-[4-(1-methylpiperidin-1-ium-1-yl)butanoylamino]ethyl] phenyl] trifluoromethanesulfonate iodide.* To a solution of compound **9** (405 mg, 0.96 mmol) in 10 mL of dry THF, 0.598 mL (9.96 mmol) of MeI were added and the solution was stirred at room temperature overnight. The solvent was removed under vacuum to give a solid that was triturated with 10 mL of *n*-hexane for 2 h. The solid was filtered and dried under vaccum at 50 °C to afford [4-[(1R)-1-[4-(1-methylpiperidin-1-ium-1-yl)butanoylamino]ethyl]phenyl] trifluoromethanesulfonate iodide as an orange solid. $[\alpha]_D^{25}$ (c = 0.15, CH_3OH): +27; ^{1}H-NMR ($CDCl_3$) δ 7.58 (bs, 1H, NH), 7.75 (d, 2H, J = 7 Hz), 7.55 (d, 2H, J = 7 Hz), 4.5 (q, 1H, J = 7 Hz), 3.65 (m, 2H), 3.45–3.05 (m, 9H), 2.85 (t, 2H, J = 3 Hz), 1.95–1.90 (m, 6H), 1.45 (s, 3H, J = 7 Hz).

In Vitro Selectivity of DF2593A. The effect of DF2593A (Tables S3 and S4) was evaluated on a panel of different GPCR (radioligand binding assays) and on ion channels (calcium assay). For radioligand binding, all of the reagents were purchased by PerkinElmer. Assays were performed according to the manufacturer's instructions. Sample radioactivity content was measured by a microplate scintillation Beta-counter Top Count NXT. The ability of each test article to act as an antagonist on three transient receptor potential (TRP) channels was evaluated in a calcium assay. For TRPV1 and TRPV4, experiments were performed with the FLIPR Fluo-8 calcium Assay Kit according to the manufacturer's instructions. For TRPM8, experiments were performed with the FLIPR Fluo-8 calcium Assay Kit according to the manufacturer's instructions (BD Bioquest).

Pharmacokinetics of DF2593A. Male C57BI/6J mice (Charles River) were fed ad libitum and housed under controlled conditions with a 12-h light-dark cycle. Procedures involving animals and their care conformed to institutional guidelines that are in compliance with national (D.L. n. 116, G.U. suppl. 40; February 18, 1992) and international laws and policies [EEC Council Directive 86/609, OJ L 358, 1; December 12, 1987; *NIH Guide for the Care and Use of Laboratory Animals* (14)]. DF2593A was dosed in PBS for oral (1 mg/kg) administration in fasted mice. Blood samples (n = 3 per time point) were harvested at different time points up to 12 h after single dose administration. For brain permeation studies, DF2593A was dosed intravenously at 10 mg/kg. Samples were analyzed by LC/MS with appropriate standards. Pharmacokinetic parameters were calculated using noncompartimental analysis with WinNonlin 6.2 (Pharsight).

Animals. The behavioral experiments were performed on male C57Bl6 mice (20–25 g) housed in the animal care facility of the School of Medicine of Ribeirao Preto. Male C5a-receptor-deficient mice ($C5aR^{-/-}$) (C.129S4-C5ar1tm1cge/J) on a BALB/C background were purchased from The Jackson Laboratory. BALB/C mice were used as control of $C5aR^{-/-}$ mice. All procedures were in accordance with the guidelines of the International Association for the Study of Pain on the use of animals in pain research.

Induction of Paw Inflammation. Mice received an intraplanta injection of carrageenin (100 μg per paw) or CFA (10 μL) injected subcutaneously into the plantar region of the hindpaw, as previously described (15, 16).

Mechanical Nociceptive Paw Test. Mechanical hyperalgesia was tested in mice as previously reported (15). The test consisted of evoking a hind paw flexion reflex with a hand-held force transducer adapted with a 0.5-mm^2 polypropylene tip (Electronic von Frey; IITC Life Science). The stimulus applied in between the five distal footpads with a gradual increase in pressure was automatically discontinued and its intensity recorded when the paw was withdrawn. The end point was characterized by the removal of the paw in a clear flinch response after the paw withdrawal. The results are expressed by the Δ withdrawal threshold (in grams) that was calculated by subtracting the average of the last three measurements after the treatments from the average of three measurements before treatments.

Leukocyte Migration to the Paw Skin Tissue. The leukocyte migration to the subcutaneous plantar tissue of mice hind paw was evaluated with the myeloperoxidase (MPO) kinetic-colorimetric assay, as previously described (17). Samples of subcutaneous plantar tissue were collected in 50 mM K_2HPO_4 buffer (pH 6.0) containing 0.5% hexadecyltrimethylammonium bromide and kept at −80 °C until use. Samples were homogenized using a Polytron (PT3100), centrifuged at 16,100 × g for 4 min, and the resulting supernatant assayed spectrophotometrically for MPO activity determination at 450 nm (Spectra max), with three readings in 1 min. The MPO activity of samples was compared with a standard curve of neutrophils. Briefly, 10 μL of sample was mixed with 200 μL of 50 mM phosphate buffer pH 6.0, containing 0.167 mg/mL *O*-dianisidinedihydrochloride and 0.0005% hydrogen peroxide.

Writhing Tests. The zymosan-induced writhing was performed as previously described (18). Briefly, zymosan (1 mg/200 μL) was injected into the peritoneal cavity of mice. These mice were placed in a large glass cylinder and the intensity of nociceptive behavior was quantified by counting the total number of writhes occurring between 0 and 20 min after stimulus injection. The writhing response consists of a contraction of the abdominal muscle together with a stretching of hind limbs. The antinociceptive activity was expressed as the writhing scores over the 20 min.

Hot-Plate Test. Mice were placed in a 10-cm-wide glass cylinder on a hot plate (IITC Life Science) maintained at 55.0 °C. Two control latencies at least 10 min apart were determined for each mouse. The reaction time was scored when the animal jumped or licked its paws. To minimize tissue damage, a maximum latency (cut-off) was set at 30 s (18).

Measurement of Motor Performance. To discard possible nonspecific muscle relaxant or sedative effects of DF2593A, mice motor performance was evaluated on the rota-rod test (18). The apparatus consisted of a bar with a diameter of 2.5 cm, subdivided into six compartments by disks 25 cm in diameter (Ugo Basile, Model 7600). The bar rotated at a constant speed of 22 rotations per minute. The animals were selected 24 h previously by eliminating those mice that did not remain on the bar for two consecutive periods of 120 s. Animals were treated orally with vehicle or DF2593A (1 mg/kg). Diazepam (7.5 mg/kg, s.c.) was used as a positive control. The cut-off time used was 120 s.

Induction of Zymosan Joint Inflammation. Joint inflammation was induced by administration of zymosan (150 μg) (Sigma) diluted in 0.9% saline into the right femur-tibial joint region of mice lightly anesthetized. The volume administered was 10 μL via a 29-G hypodermic needle inserted into the joint. Control animals received a single intra-articular injection of the same volume of sterile saline (19).

Antigen-Induced Arthritis. Mice were immunized as described previously (20). Briefly, mice were sensitized with 500 μg of methylated BSA (mBSA) in 0.2 mL of an emulsion containing 0.1 mL saline and 0.1 mL CFA (1 mg/mL of *Mycobacterium tuberculosis*) and given by subcutaneous injection on day 0. The mice were boosted with the same preparation on day 7. Twenty-one days after the initial injection, arthritis was induced in the immunized animals by intra-articular injection of mBSA (30 μg per cavity) dissolved in 10 μL of saline into the right femur-tibial joint (20).

Articular Nociception. Articular nociception during zymosan and antigen-induced arthritis was evaluated as previously described (19, 20). For this test, a polypropylene tip probe with an area size of 4.2 mm^2 that was adapted to a hand-held force transducer, instead of the standard tip probe (0.5 mm^2), was applied on the plantar surface of a hind paw to produce a tibio-tarsal flexion movement. An increasing perpendicular force was applied to the central area of the plantar surface of the hind paw to induce a dorsal flexion of the tibio-tarsal joint, followed by paw withdrawal. A tilted mirror below the grid provided a clear view of the animal's hind paw. The electronic pressure-meter apparatus automatically recorded the intensity of the force applied when the paw was withdrawn. The test was repeated until three subsequently consistent measurements were obtained (i.e., the variation among these measurements was less than 2 g). The flexion-elicited withdrawal threshold is expressed in grams.

Thermal Nociceptive Test. The latency of paw withdrawal to radiant heat stimuli was measured using a Plantar Ugo Basile apparatus (Stoelting), as previously described (21). Mice can move freely in this apparatus on an elevated glass surface with plastic boxes above as the top cover. Mice were given a 1-h acclimation period before testing until they became calm and motionless. A calibrated infrared light source of high intensity was applied perpendicular on the plantar surface of each mouse's hind paw. The end point was characterized by the removal of the paw followed by clear flinching movements. Latency to paw withdrawal was automatically recorded. Each hind paw was tested alternately with an interval of 5 min for four trials.

SNI-Induced Neuropathic Pain-Like Behavior. Under isoflurane (2%) anesthesia, the skin on the lateral surface of the thigh was incised and a section made directly through the biceps femoris muscle exposing the sciatic nerve and its three terminal branches: the sural, common peroneal, and tibial nerves. The SNI procedure comprised an axotomy and ligation of the tibial and common peroneal nerves, leaving the sural nerve intact. The common peroneal and the tibial nerves were tight-ligated with 5.0 silk and sectioned distal to the ligation, removing 2 ± 4 mm of the distal nerve stump. Muscle and skin were closed in two layers (22).

Data Analyses and Statistics. For in vivo experiments, results are presented as mean ± SEM. The differences among the groups were compared by ANOVA (one-way) and individual comparisons were subsequently made with Bonferroni's post hoc test. The level of significance was set at $P < 0.05$.

1. Bertini R, et al. (2004) Noncompetitive allosteric inhibitors of the inflammatory chemokine receptors CXCR1 and CXCR2: Prevention of reperfusion injury. *Proc Natl Acad Sci USA* 101(32):11791–11796.
2. Imai T, et al. (1998) Macrophage-derived chemokine is a functional ligand for the CC chemokine receptor 4. *J Biol Chem* 273(3):1764–1768.
3. Bertini R, et al. (2012) Receptor binding mode and pharmacological characterization of a potent and selective dual CXCR1/CXCR2 non-competitive allosteric inhibitor. *Br J Pharmacol* 165(2):436–454.
4. Munson PJ, Rodbard D (1980) Ligand: A versatile computerized approach for characterization of ligand-binding systems. *Anal Biochem* 107(1):220–239.
5. Bizzarri C, et al. (2001) Selective inhibition of interleukin-8-induced neutrophil chemotaxis by ketoprofen isomers. *Biochem Pharmacol* 61(11):1429–1437.
6. Edgar RC (2004) MUSCLE: multiple sequence alignment with high accuracy and high throughput. *Nucleic Acids Res* 32(5):1792–1797.
7. Fredriksson R, Lagerström MC, Lundin LG, Schiöth HB (2003) The G-protein-coupled receptors in the human genome form five main families. Phylogenetic analysis, paralogon groups, and fingerprints. *Mol Pharmacol* 63(6):1256–1272.
8. Allegretti M, et al. (2005) Targeting C5a: Recent advances in drug discovery. *Curr Med Chem* 12(2):217–236.
9. Beato C, Beccari AR, Cavazzoni C, Lorenzi S, Costantino G (2013) Use of experimental design to optimize docking performance: The case of LiGenDock, the docking module of LiGen, a new de novo design program. *J Chem Inf Model* 53(6):1503–1517.
10. Beccari AR, Cavazzoni C, Beato C, Costantino G (2013) LiGen: A high performance workflow for chemistry driven de novo design. *J Chem Inf Model* 53(6):1518–1527.
11. Moriconi A, et al. (2007) Design of noncompetitive interleukin-8 inhibitors acting on CXCR1 and CXCR2. *J Med Chem* 50(17):3984–4002.
12. Aureli L, et al. (2005) Predicting human serum albumin affinity of interleukin-8 (CXCL8) inhibitors by 3D-QSPR approach. *J Med Chem* 48(7):2469–2479.
13. Monk PN, Pease JE, Marland G, Barker MD (1994) Mutation of aspartate 82 of the human C5a receptor abolishes the secretory response to human C5a in transfected rat basophilic leukemia cells. *Eur J Immunol* 24(11):2922–2925.
14. US National Research Council (1996) *NIH Guide for the Care and Use of Laboratory Animals* (National Academy Press, Washington, DC).
15. Cunha TM, et al. (2004) An electronic pressure-meter nociception paw test for mice. *Braz J Med Biol Res* 37(3):401–407.
16. Valério DA, et al. (2007) Anti-inflammatory and analgesic effects of the sesquiterpene lactone budlein A in mice: Inhibition of cytokine production-dependent mechanism. *Eur J Pharmacol* 562(1-2):155–163.
17. Cunha TM, et al. (2008) Dual role of hydrogen sulfide in mechanical inflammatory hypernociception. *Eur J Pharmacol* 590(1-3):127–135.
18. Ribeiro RA, et al. (2000) Involvement of resident macrophages and mast cells in the writhing nociceptive response induced by zymosan and acetic acid in mice. *Eur J Pharmacol* 387(1):111–118.
19. Guerrero AT, et al. (2006) Hypernociception elicited by tibio-tarsal joint flexion in mice: A novel experimental arthritis model for pharmacological screening. *Pharmacol Biochem Behav* 84(2):244–251.
20. Pinto LG, et al. (2010) IL-17 mediates articular hypernociception in antigen-induced arthritis in mice. *Pain* 148(2):247–256.
21. Hargreaves K, Dubner R, Brown F, Flores C, Joris J (1988) A new and sensitive method for measuring thermal nociception in cutaneous hyperalgesia. *Pain* 32(1):77–88.
22. Decosterd I, Woolf CJ (2000) Spared nerve injury: An animal model of persistent peripheral neuropathic pain. *Pain* 87(2):149–158.

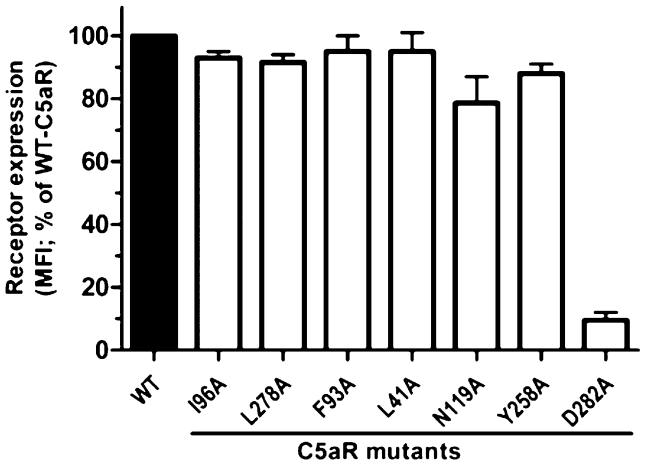

Fig. S1. Expression levels of C5aR mutants. Cell surface expression of WT (black column) and indicated point mutants (white columns) of C5aR transiently transfected in L1.2 cells. Results are mean ± SEM of three independent experiments. D282A-C5aR is the only mutant significantly impaired compared with WT C5aR ($P < 0.01$).

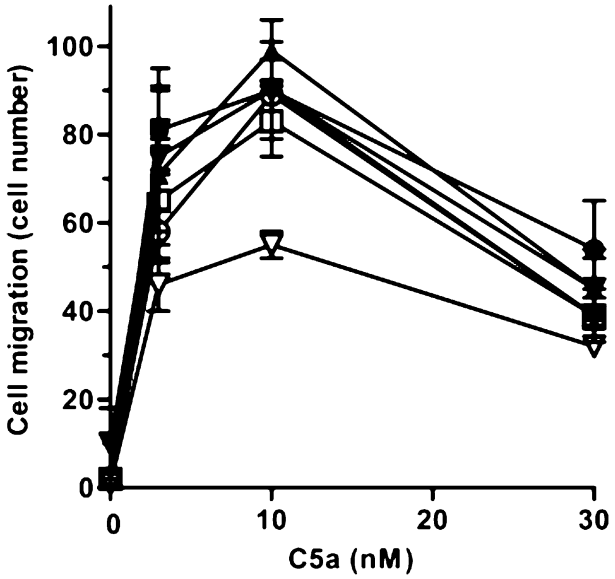

Fig. S2. Chemotactic activity of C5aR mutants toward C5a. Chemotactic activity of increasing doses of C5a on the migration of wt (●), L41A (○), F93A (□), I96A (▲), L278A (▼), N119A (▽), and Y258A (■) C5aR/L1.2 transfectants. Results are mean ± SEM of three independent experiments. A significant difference ($P < 0.05$) was only observed for N119A-C5aR/L1.2 at 10 nM C5a.

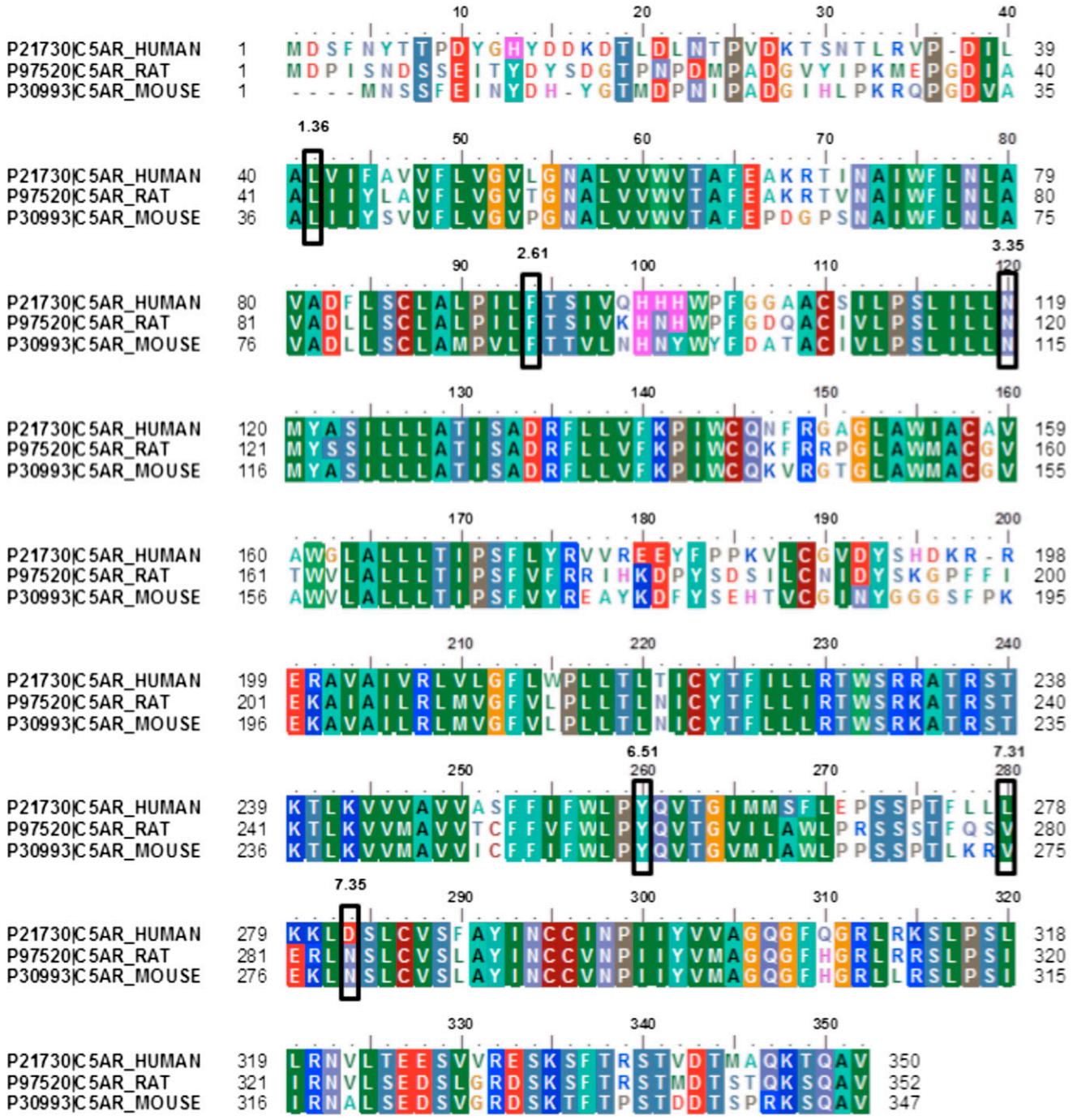

Fig. S3. Sequence alignment of human, mouse, and rat C5aR. Asn120$^{3.35}$ and Tyr258$^{6.51}$ are fully conservatively in the C5aR orthologs, whereas Asp282$^{7.35}$ is replaced by Asn$^{7.35}$ in both the orthologs. Hydrophobic residues, Leu41$^{1.36}$ and Phe93$^{2.61}$ are also fully conserved in mouse and rat C5aR. Ile96$^{2.64}$ is conserved in rat (Ile97$^{2.64}$) and is replaced by Val92$^{2.64}$ in mouse C5aR. Leu278 $^{7.31}$ is replaced by a similar hydrophobic residue, Val275$^{7.31}$ and Val280$^{7.31}$ in mouse and rat, respectively. Key residues of the allosteric pocket are shown in black boxes with Weinstein–Ballesteros annotation. Uniprot ID codes are provided.

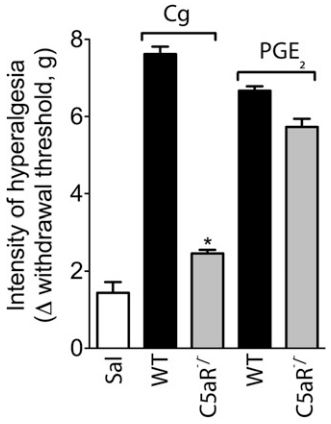

Fig. S4. Inflammatory hyperalgesia induced by carrageenan (Cg), but not by PGE_2, is reduced in C5a-null mice. WT or $C5aR^{-/-}$ mice received intraplantar injection of Cg (100 μg per paw), PGE_2 (100 ng per paw), or saline. At 3 h mechanical hyperalgesia was determined. Data are shown as mean ± SEM; $*P < 0.05$ when compared with wild type group; $n = 6$.

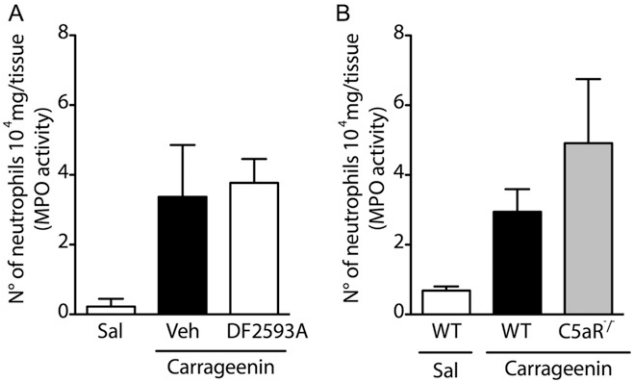

Fig. S5. Role of C5a in neutrophil migration during Cg-induced inflammation in mice paw. (*A*) Effect of DF2593A on the Cg-induced increase in paw MPO activity. Mice were treated orally with vehicle (saline) or DF2593A (1 mg/kg) 50 min before intraplantar injection of Cg (100 μg per paw). MPO activity (number of neutrophils 10^4/mg tissue) was evaluated in the plantar tissue 5 h after Cg injection. (*B*) WT and $C5aR^{-/-}$ mice receive an intraplantar injection of Cg (100 μg per paw). MPO activity (number of neutrophils 10^4/mg tissue) was evaluated in the plantar tissue 3 h after Cg injection. Data are shown as mean ± SEM $n = 6$.

Table S1. Sequence alignment of key polar residues among CXCR1/2 and C5aR

	Pocket polar residues			
Receptor (Uniprot ID)	3.35	6.51	7.35	7.39
CXCR1 (P25024)	N120	Y258	L287	E291
CXCR2 (P25025)	N129	Y267	L296	E300
C5AR (P21730)	N119	Y258	D282	V286

Two of the three key polar residues ($Asn120^{3.35}$, $Tyr258^{6.51}$, and $Glu291^{7.39}$) of CXCR1 are conservatively replaced ($Asn119^{3.35}$ and $Tyr258^{6.51}$) in C5aR, whereas the lack of the glutamate in position 7.39 ($Val286^{7.39}$ in C5aR) is compensated by $Asp282^{7.35}$. Uniprot ID codes are provided in parenthesis. Amino acids are color coded by type: red, acidic residues; green, hydrophobic aliphatic residues; blue, aromatic residues; violet, noncharged polar residues.

Table S2. Effect of selected molecules on CXCL8-, CXCL1-, and C5a-induced human PMN chemotaxis

Compound	Structure	CXCL8	CXCL1	C5a
1	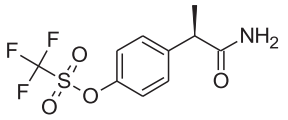	8 ± 0.6	26 ± 2.3	>10,000
2	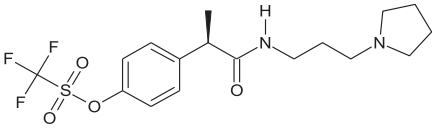	5 ± 0.2	20 ± 1.1	50 ± 3.4
3	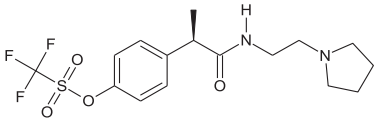	10 ± 0.3	30 ± 2.2	60 ± 4.2
4	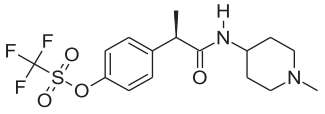	>10,000	>10,000	50 ± 3.2
5	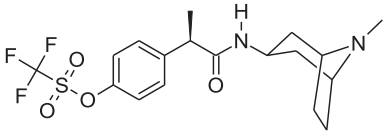	>10,000	>10,000	60 ± 1.2
6	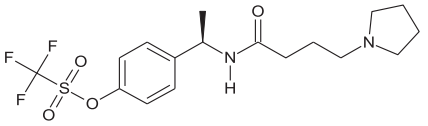	>10,000	>10,000	40 ± 2.3
7	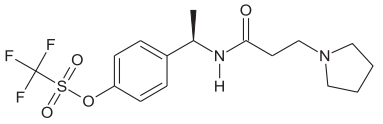	>10,000	>10,000	300 ± 19
8	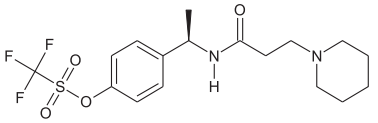	>10,000	>10,000	150 ± 10
9	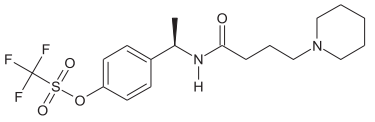	>10,000	>10,000	5 ± 1.3
10	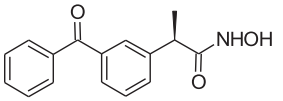	>10,000	>10,000	10 ± 1.1
11	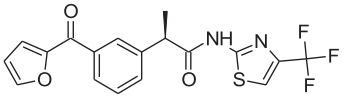	>10,000	>10,000	10 ± 0.8
12	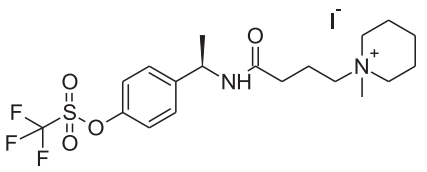	>10,000	>10,000	10 ± 0.6

For CXCL8, CXCL1, and C5a, IC_{50} in nM (± SD).

Table S3. Selectivity of DF2593A in a panel of different GPCRs

GPCR	Ligand	Mean ± SD
α_{1A}-adrenoreceptor	[^{125}I]-HEAT	105.0 ± 5.7
α_{2A}-adrenoreceptor	[^{3}H]-Rawolscine	88.5 ± 2.8
β_1-adrenoreceptor	[^{3}H]-CGP12177	95.3 ± 14.2
β_2-adrenoreceptor	[^{3}H]-CGP12177	97.3 ± 5.9
B_1	[^{3}H]-(des-Arg^{10},Leu^{9})-Kallidin	95.5 ± 6.9
B_2	Bradykinin	98.5 ± 6.0
CB1	[^{3}H]-CP-55,940	92.5 ± 5.8
CB2	[^{3}H]-CP-55,940	88.5 ± 13.4
D2	[^{3}H]- Methylspiperone	91.7 ± 1.0
D3	[^{125}I]-7-OH-PIPAT	85.4 ± 2.3
H1	[^{3}H]-Pyrilamine	62.7 ± 0.7
H2	[^{125}I]-Aminopotentidine	98.0 ± 9.31
M2*	[^{3}H]-*N*-methyl scopolamine	10.1 ± 0.8 (10 μM)
		60.1 ± 1.1 (1 μM)
		100.1 ± 5.1 (0.1 μM)
		15.3 ± 0.7 (10 μM)
M3*	[^{3}H]-*N*-methyl scopolamine	55.1 ± 3.4 (1 μM)
		95.4 ± 3.0 (0.1 μM)
NK_1	[^{125}I]-Substance P	92.5 ± 0.7
μ	[^{3}H]-DAMGO	90.4 ± 3.1
κ	[^{3}H]-U69,593	88.4 ± 3.0
δ	[^{3}H]-Naltrindole	94.1 ± 14.9
NOP	[^{3}H]-Nociceptin	110.6 ± 2.9
5-HT1A	[^{3}H]-8-Hydroxy-DPAT	97.3 ± 17.8

Data are presented as mean (± SD, n = 3) of the percent of binding of radioligand after the incubation with DF2593A at the single concentration of 10 μM.

*The effect of DF2593A was evaluated at 10, 1 and 0.1 μM. DF2593A retains about 1,000-fold of selectivity versus M2 and M3.

Table S4. Selectivity of DF2593A in a panel of different ion channels

Ion channel	Ligand	IC_{50} (μM)
TRPM8	Icilin	>10
TRPV1	Capsaicin	>10
TRPV4	GSK1016790A	>10

For TRPM8, TRPV1, and TRPV4 experiments, data are presented as IC_{50} values of three different experiments.